CR-161768

**RADIO SCIENCES COMPANY** SPACE • MAGNETOSPHERE • IONOSPHERE • ATMOSPHERE

624 TULANE AVENUE
MELBOURNE, FLORIDA 32901
TELEPHONE: (305) 723-7425

RSCR-81-2

(NASA-CR-161768) NOISE AND INTERFERENCE STUDY FOR SATELLITE LIGHTNING SENSOR Final Report, Apr. 1980 - Apr. 1981 (Radio Sciences Co., Melbourne) 74 p HC A04/MF A01 CSCL 20A G3/32

N81-25281

Unclas
42446

# NOISE AND INTERFERENCE STUDY FOR SATELLITE LIGHTNING SENSOR

Final Report

on

Contract NAS8-33891

Period Covered: April 1980 - April 1981

John R. Herman
Principal Investigator

May 6, 1981

Prepared for:

NASA George C. Marshall Space Flight Center
Marshall Space Flight Center
Alabama 35812

## ABSTRACT

The use of radio frequency techniques for the detection and monitoring of terrestrial thunderstorms from space requires assessment of three major points: (1) the lightning and noise source characteristics; (2) propagation effects imposed by the atmosphere and ionosphere; and (3) the electromagnetic environment in near space within which lightning rf signatures must be detected. A composite frequency spectrum of the peak rf amplitude from lightning flashes is developed for a ground observer from a variety of reported measurements. Propagation effects, including ionospheric cutoff, refraction, absorption, dispersion and scintillation, are then considered for modifying the lightning spectrum to the geosynchronous case. Comparison of the modified spectrum with interfering noise source spectra suggest, somewhat surprizingly, that rf lightning pulses on frequencies up to a few GHz should be detectable above the natural noise environment in near space. The spatial resolution for locating lightning flashes by rf techniques on space platforms is expected to be relatively poor.

ACKNOWLEDGEMENTS

We are pleased to acknowledge helpful discussions with a number of colleagues during the course of this investigation: Profs. Tom Shumpert and Martial Honnell of Auburn University; Mssrs. F.W. Wagnon and J.W. Harper of Marshall Space Flight Center; Dr. W.W. Vaughan, MSFC; Mr. W.L. Taylor and Dr. W.D. Rust, NOAA Severe Storms Laboratory; Prof. E.P. Krider, University of Arizona; and Prof. A.A. Few, Rice University. Also, we are grateful to C.T. Herman, Radio Sciences Company, for computer programming and analysis support throughout the contract, and to H.C. Herman, Radio Sciences Company, for executing some of the figures for this report.

TABLE OF CONTENTS

LIST OF ILLUSTRATIONS

## 1. INTRODUCTION

At a recent NASA-sponsored workshop to examine the need for lightning observations from space (Christensen et al, 1979), it was decided that detection and monitoring of terrestrial thunderstorm activity from space is of interest from both scientific and practical points of view. Further, it was concluded that the best technique for measuring the associated lightning activity will involve detection of the electromagnetic radiation produced by the lightning discharge. The spectrum of this radiation ranges from DC through radio frequencies to visible light, and thus offers a variety of options for instrumentation development. Instrumentation techniques for the optical and radio frequency (rf) portions of the spectrum are so different, however, that it is convenient to consider them separately. The present investigation has concerned itself only with the radio aspect of lightning detection from space.

It has been recognized from the outset that in order to specify design requirements for an rf lightning detection system, three major points need to be considered: (1) the lightning and noise source characteristics; (2) propagation effects imposed by the atmosphere, ionosphere and magnetosphere on the lightning signatures; and (3) the background electromagnetic environment in near space within which lightning signatures must be detected. Details of the major points are identified in Fig. 1, although not all of them are treated explicitly in this final report. Rather, the present study has addressed the major factors, in order to establish a body of information which may serve as a basis

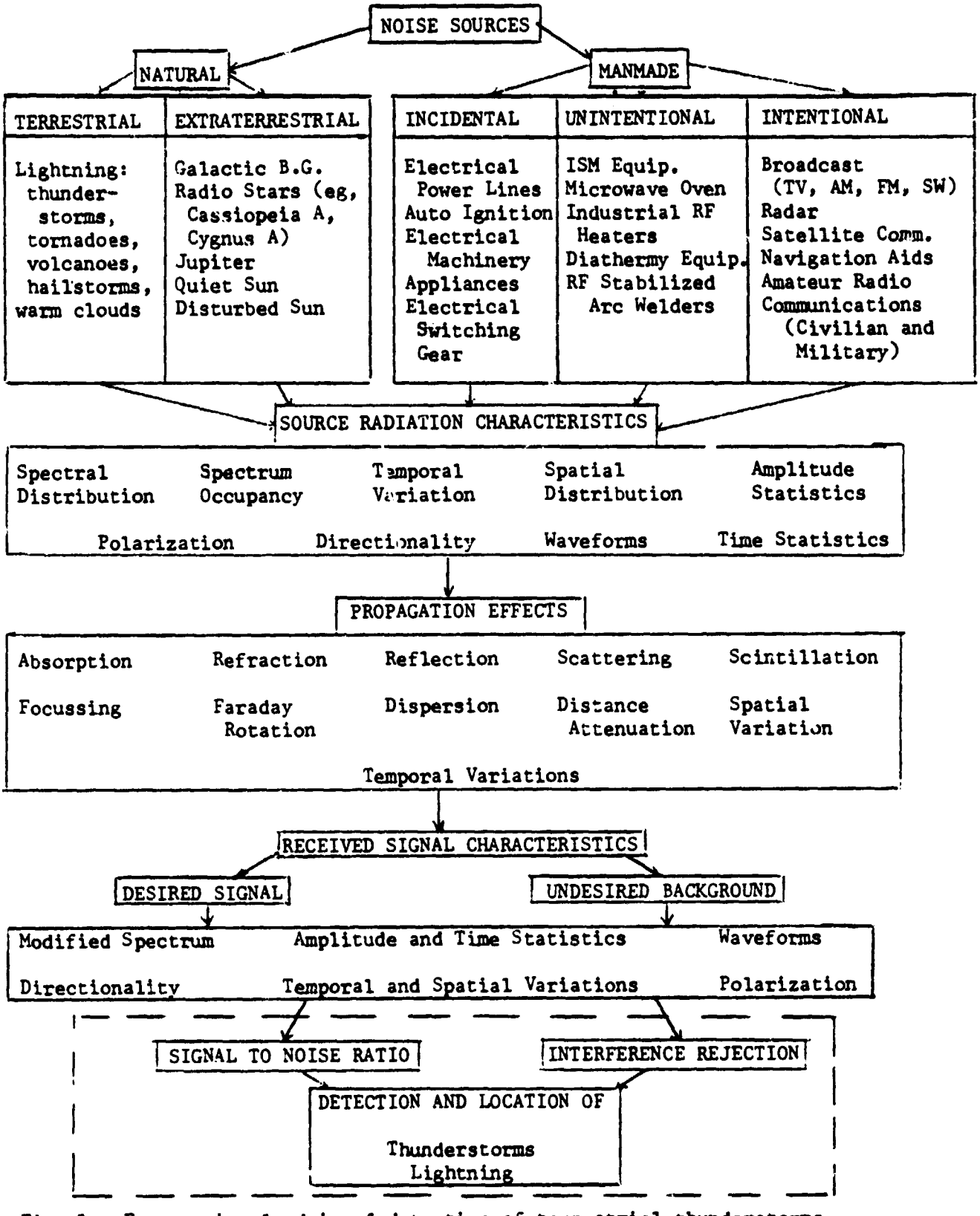


Fig. 1. Factors involved in rf detection of terrestrial thunderstorms using a space platform.

for definition of the design and operational requirements of a system using rf signals to detect, locate and characterize lightning discharges. The study should not be considered as complete; additional investigation would be desirable if a program is established to seriously consider use of space platforms for rf lightning investigations.

In this report, section 2 describes the rf lightning signature as observed at the ground, section 3 considers the space/surface geometry involved, and section 4 summarizes some expected propagation effects preparatory to deriving a modified lightning spectrum that might be seen above the ionosphere. Section 5 presents the modified spectrum along with a description of the noise and interference environment in near space. Comparison of the signal and noise spectra (section 5.4) indicates that a lightning signature may be visible above the noise on frequencies out to a few GHz at geosynchronous height. Conclusions are stated in section 6, and references cited are collected alphabetically in section 7.

## 2.0 RF LIGHTNING SIGNATURES

To better use rf radiation of the lightning flash for detection purposes, it is helpful to understand the physical characteristics of the flash itself, its relationship to thunderstorm activity, and the statistics of thunderstorm occurrence. These topics are taken up below.

### 2.1 The Lightning Flash

Lightning discharges with significant associated rf radiation are characterized by type as cloud-to-ground, cloud-to-cloud, and intra-cloud. From a broadly practical viewpoint, the cloud-to-ground discharge is the most important for it is this type that causes personal injury and property damage; it has therefore received the most detailed study and is relatively well understood.

The structure of the cloud-to-ground flash (e.g., Fig. 2) has been deduced from optical and radio observations, and it appears that different portions of the rf spectrum are generated by different parts of the flash. The sequential development of the total discharge apparently begins with a "pilot streamer" followed by the "stepped leader" down the stem of the pilot streamer (Chalmers, 1967). The stepped leader may have a number of branches (see Fig. 2), and as soon as one of them reaches the Earth it opens an ionized path for the "return stroke" (main stroke) to quickly drain the charge in the leader to the Earth. For subsequent strokes the stepped leader is replaced by a "dart leader". A total cloud-to-ground discharge may have as little as one main

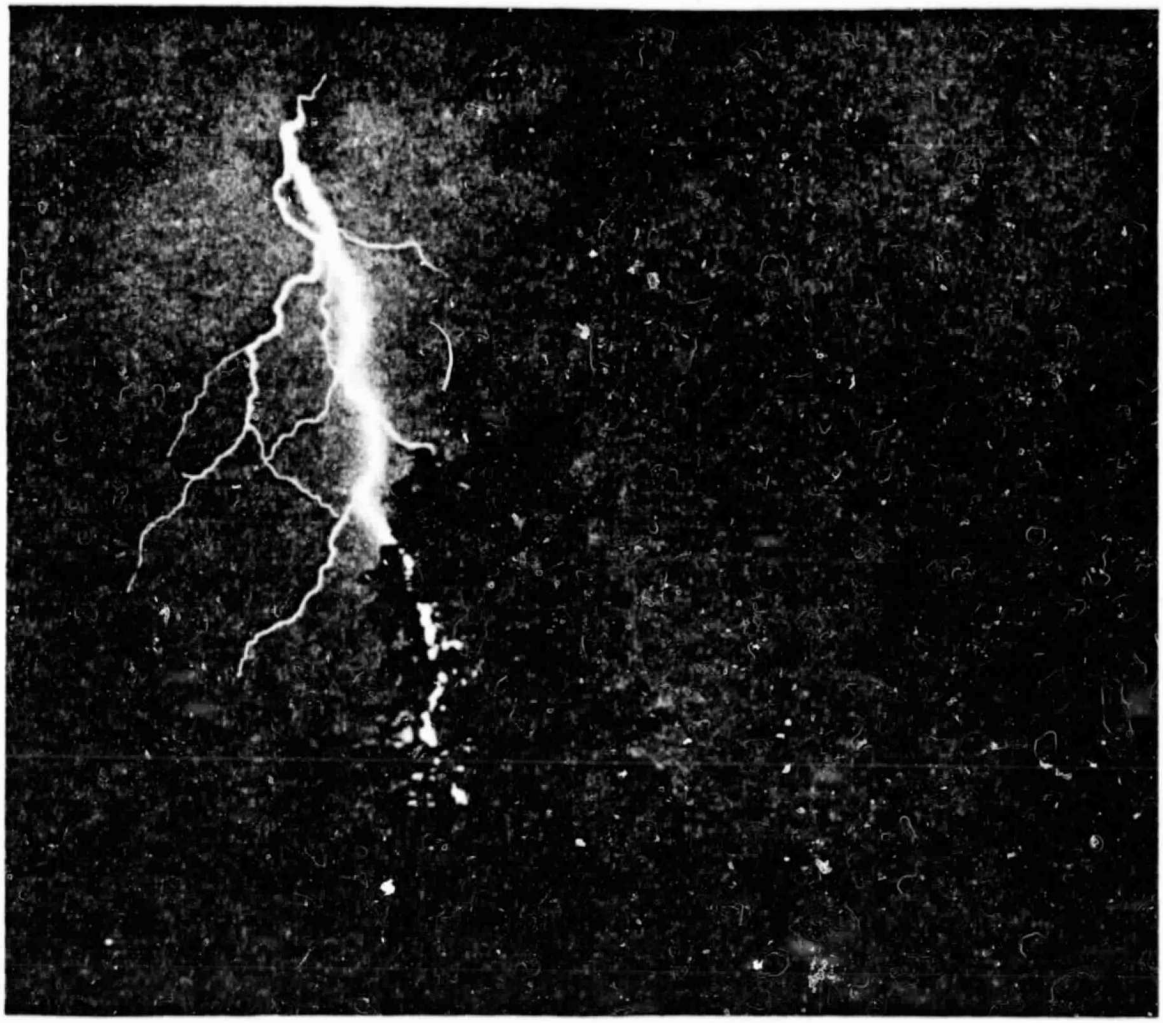

Fig. 2. Typical cloud-to-ground lightning flash photographed by Richard Orville (Christensen et al, 1979).

stroke up to as many as nine or ten return strokes (Hewitt, 1962). In between return strokes and sometimes after the final stroke, K changes will occur. Pierce (1969) has defined the K change thusly: "If an advancing charge-carrying leader encounters a concentration of charge of opposite sign, there is a rapid recoil surge of current backwards along the advancing channel. ...the phenomena accompanying the sudden surges are described as K changes."

A similar structure apparently exists in intra-cloud and cloud-to-cloud flashes as well, except there is no true return stroke (Pierce, 1969), and K changes are more pronounced. Also, the rf radiation characteristics are not the same for cloud-to-ground and intra-cloud flashes.

## 2.2 RF Radiation from Lightning

The rf radiation from a lightning discharge varies with frequency, both as to the number of pulses and to the timing of occurrence within the discharge duration. The pulses from a single discharge observed with narrowband receivers tuned to frequencies between 10 kHz and 10 MHz are shown in Fig. 3. Note that at VLF (3-30 kHz) the pulses are discrete and associated with return strokes or recoil streamers (K changes), and the number of pulses increases with increasing frequency, till at high frequencies the emission is quasi-continuous. There appears to be a temporary secession in the 1- and 10-MHz radiation from the ground flash just after the two return strokes; this is not evident in the cloud discharge. The number of pulses per flash maximizes at about $10^4$ in the VHF band (not shown), but then begins to decrease again

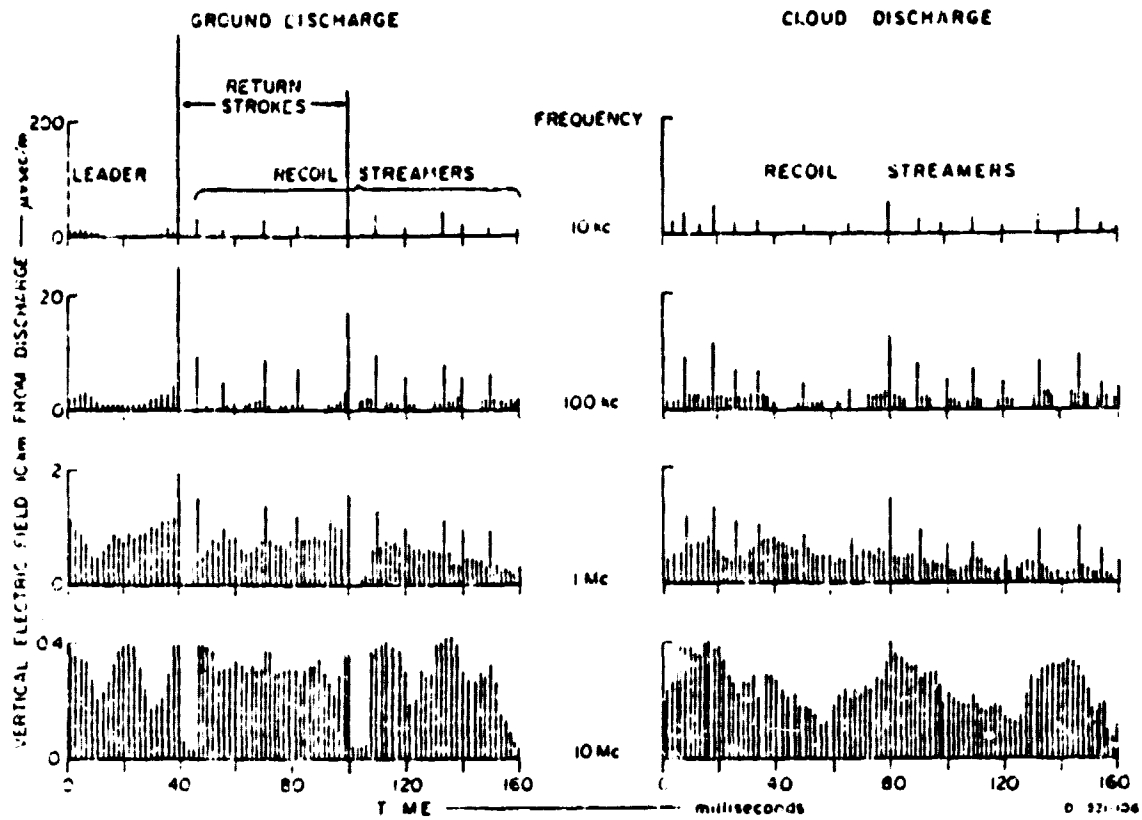


Fig. 3. Pulse structure of close cloud-to-ground and intracloud lightning flashes observed with narrow band receivers (Pierce, 1969).

until in the GHz range the pulses are discrete and are again associated with return strokes and K changes. There is some evidence that strong noise on 600 MHz is generated by cloud flashes (Hewitt, 1962), similar to leader processes, but Oetzel (see Oetzel and Pierce, 1969) found that at 11 GHz almost all of the radiation was associated with the return stroke (see Fig. 4). On a few occasions microwave bursts were observed in conjunction with leaders, but their intensities were an order of magnitude less.

## 2.3 Lightning Waveforms

The waveforms of lightning rf radiation have an interesting variety of shapes, of which the examples in Fig. 4 are only a small sample. The VLF waveshape of Fig. 4 for a return stroke is similar to Taylor's (1963) "group 1+" (see Fig. 5b). By contrast, the 11 GHz pulse is extremely narrow, but also positive going (Fig. 4). In Fig. 5, zero μsec marks the beginning of the return stroke, and it can be seen that the return stroke pulse can be either positive-going (Groups 1+ and 2+) or negative-going (Groups 1- to 5-). According to Taylor, Group 1+ represents the waveforms most often observed from lightning strokes. About 86% of all the atmospherics recorded by him fall into Groups 1 and 2 positive and negative.

An example of a positive-going return stroke pulse at 3 MHz is shown in Fig. 6 (LeVine and Krider, 1977). Note that the radiation amplitude builds slower and persists longer than the field change itself. Another example of a positive-going return stroke pulse for

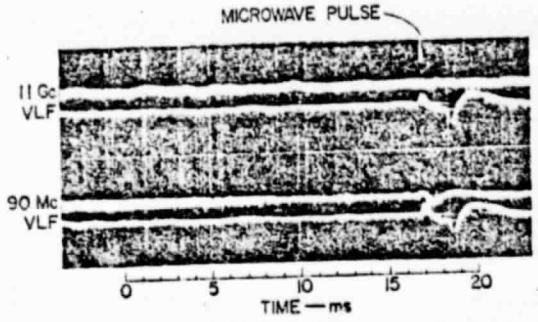


Fig. 4. Radiation waveforms simultaneously recorded on VLF, 90 MHz and 11 GHz (Oetzel and Pierce, 1969).

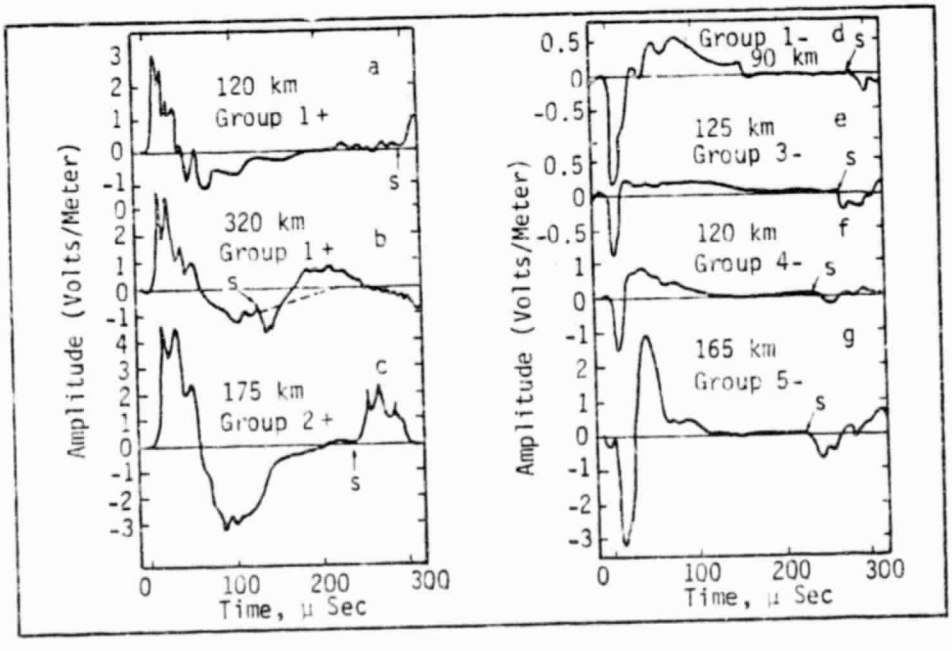


Fig. 5. Examples of atmospheric waveforms measured with broadband equipment (Taylor, 1963). Arrow labeled "s" marks time of arrival of first-hop skywave. Distance to flash indicated in km.

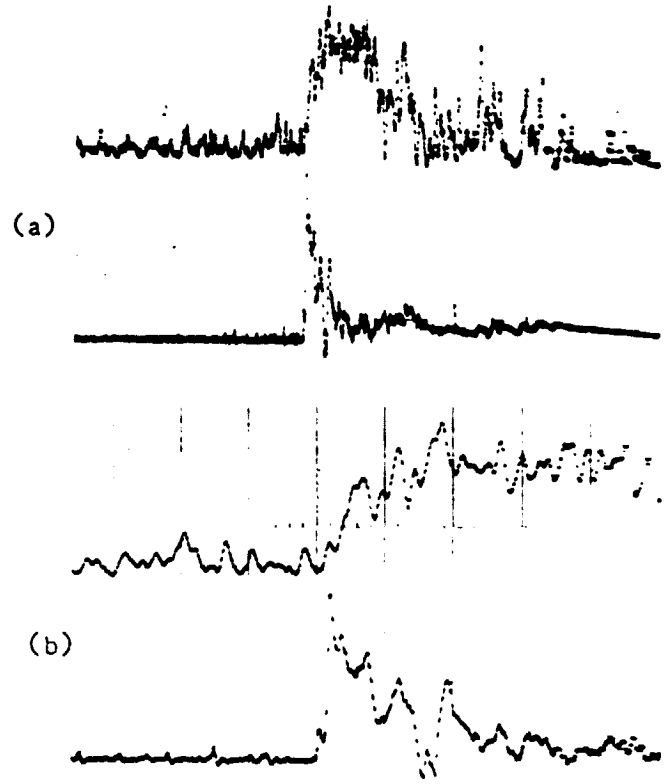


Fig. 6. Simultaneous oscilloscope records of first return stroke radiation on 3 MHz (top trace) and DC electric field change (bottom trace). Time base per large division is 100 μsec in (a) and 20 μsec in (b) (LeVine and Krider, 1977).

139 MHz is given in Fig. 7. Again note the delay in the rf peak amplitude compared to the electric field change. According to LeVine and Krider (1977), "large rf emissions do not occur until tens of microseconds after the onset of the first return strokes." The situation appears to be different for subsequent return strokes, however, as indicated in Fig. 8. In this case, it appears that the (295 MHz) rf radiation reaches maximum amplitude prior to that for the electric field change.

Similar time displacements have been observed by Rust et al (1979). Measurements of the electric field change ($\Delta E$) and rf radiation on 2200 MHz, 283 MHz and 30-50 MHz were made during a lightning flash with two return strokes. The situation for the first return stroke is given in Fig. 9, and that for the second (or subsequent) return stroke is shown in Fig. 10. In Fig. 9, note that no rf radiation is observed on 2200 MHz prior to the occurrence of the first return stroke, but on all three frequencies a strong pulse is observed to begin nearly coincidentally with the onset of the return stroke. A second pulse appears about 1 msec later, near the time of what appears to be a continuing current surge. Low intensity radiation is observed on the two lower frequencies in conjunction with the stepped leader (no field change is observed here, though), prior to the onset of the first return stroke.

For the second return stroke (R2 in Fig. 10), a strong pulse occurs on all three frequencies prior to the onset of the stroke, nearly coincident with the beginning of the dart leader (D in Fig. 10). The noise pulse is most narrow at 2200 MHz and becomes successively broader with

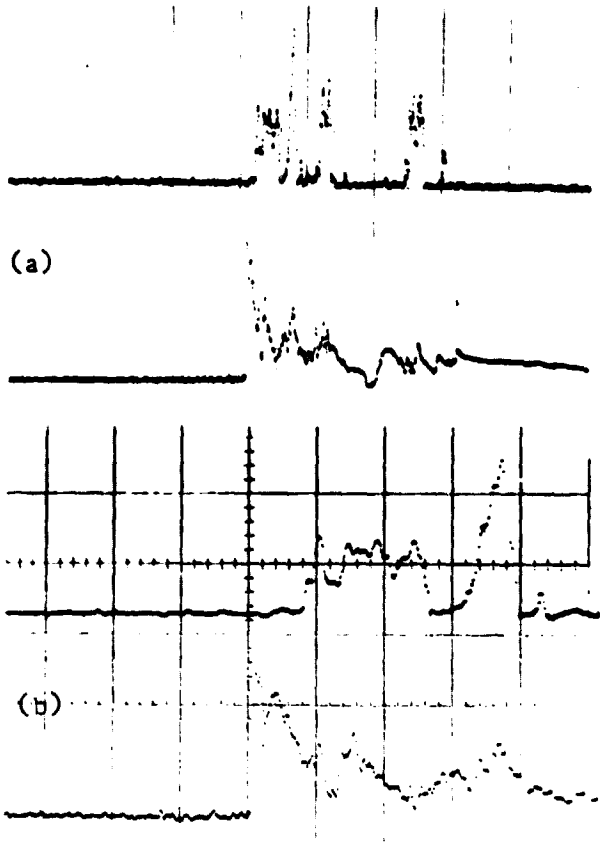


Fig. 7. Oscilloscope waveforms of first return stroke electric field change (bottom trace) and 139 MHz radiation (top trace). Time base per large division; (a) 100 μsec, (b) 20 μsec (LeVine and Krider, 1977).

Fig. 8. Simultaneous records of 295 MHz (top) and electric field change (bottom) due to subsequent return stroke. 1 large division = 100 μsec (LeVine and Krider, 1977).

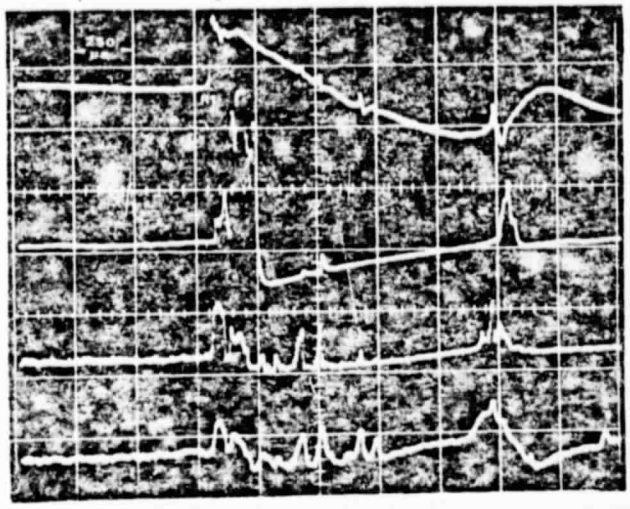


Fig. 9. Electric field change with 100 μsec relaxation time constant and radiation waveforms associated with first return stroke as observed by Rust et al (1979).

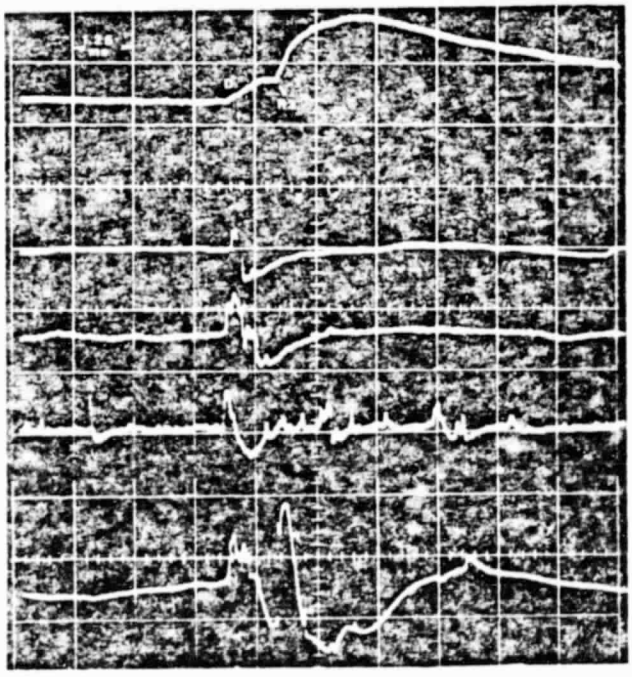


Fig. 10. Electric field changes with 3 msec and 100 μsec relaxation time constants compared to radiation waveforms associated with second return stroke of same flash as Fig. 9 (Rust et al, 1979).

decreasing frequency.

Finally, a negative-going waveform with a positive overshoot associated with a return stroke as measured by LeVine (1979) is illustrated in Fig. 11 (bottom trace). The rf pulse (top trace) is used to trigger the waveform recorder, and this result shows that strong negative-going VHF rf pulses occur prior to the initiation of a return stroke. Additional results by LeVine (1979) indicate that the strongest sources of HF and VHF radiation are associated with cloud processes occurring both before and after the first return stroke but not with the return strokes themselves. These results are compatible with Pierce's (1969) observations displayed in Fig. 3 (i.e., the 1- and 10-MHz ground stroke data). LeVine suggests that the fast negative pulses (10 $\mu$sec or less) may be associated with rapid K changes.

In summary, it appears that low frequency radiation is principally associated with return strokes, and the higher frequency radiation stems from other discharge processes, including fast K changes, continuing currents, and dart leaders.

## 2.4 Frequency Spectrum of Lightning

At the 6th International Conference on Atmospheric Electricity, Manchester, England, July 1980, Marx Brook observed that one of the greatest lacks in atmospheric electricity knowledge is a good spectrum of lightning. As discussed in the above section, it is evident that the emissions in different portions of the spectrum are generated by different processes in the lightning discharge and do not necessarily

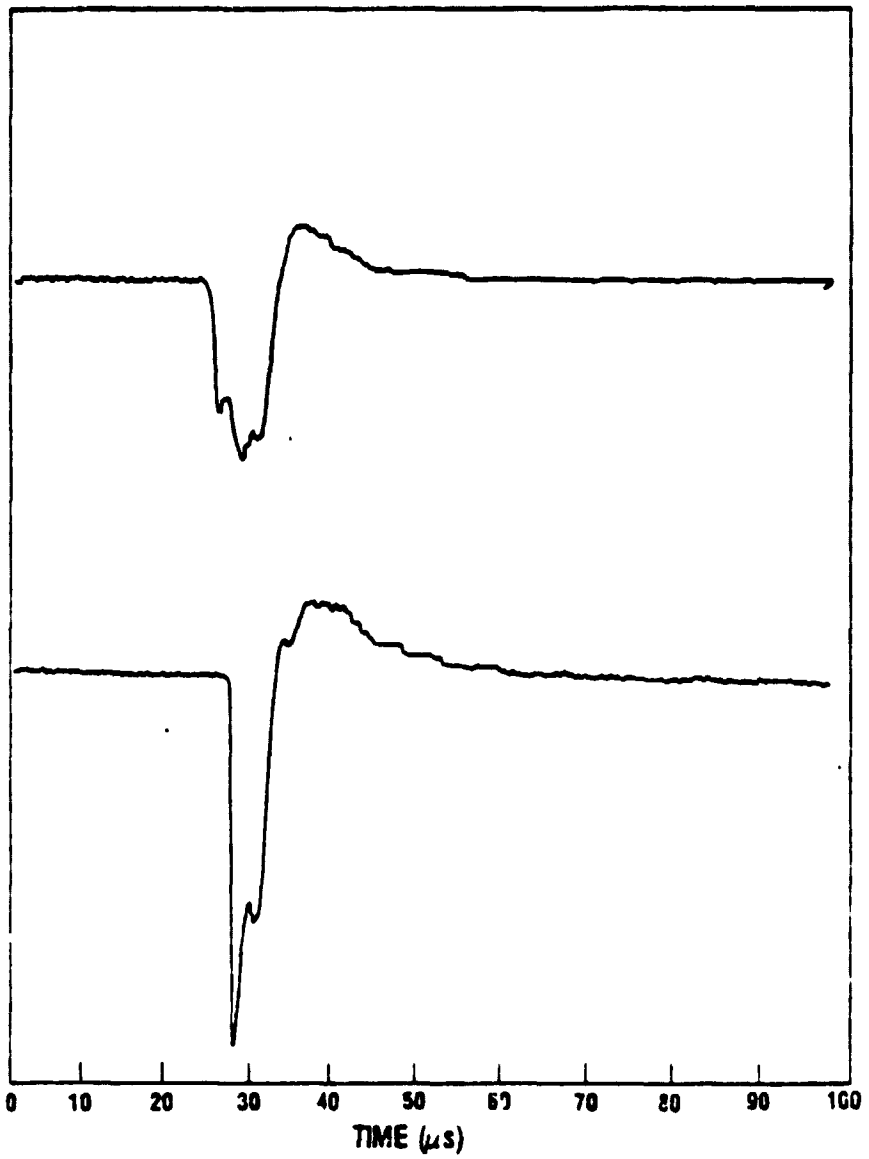


Fig. 11. Electric field change (bottom trace) triggered by 139-MHz radiation pulse (top trace). Direction of negative field change is downward (LeVine, 1979).

radiate simultaneously across the entire rf spectrum. Thus, it appears that there may be no such thing as a single lightning rf spectrum. Nevertheless, many attempts have been made to derive one through measurement and semi-theoretical techniques.

Although most earlier efforts seem to have been directed toward the VLF spectrum associated with the return stroke (e.g., Taylor, 1963; Dennis and Pierce, 1964; Hill, 1966), there have been several attempts to obtain a composite total flash spectrum over the frequency range from VLF to a few GHz (e.g., Horner, 1962; Oh, 1969; Oetzel and Pierce, 1969). A summary of these efforts is given in Fig. 12. The "x" data points between 1 kHz and 100 kHz were averaged from spectra reported by Taylor (1963) and Dennis and Pierce, 1964). Taylor's spectrum, being already an average of 47 selected "normal type" (i.e., positive going) waveforms representing 86% of all the atmospherics recorded at close range ($< 500$ km), was given double weight in the averaging for Fig. 12. The filled circles from 100 kHz to 10 GHz are linearly-equispaced averages of data from a variety of sources as reported by Oetzel and Pierce (1969). A recent measurement at 2200 MHz by Rust et al (1979) is marked by a circled x. The vertical bars through the points at decadel intervals show the data extremes rather than standard deviations. Theoretical spectra of the return stroke radiation (Bruce and Golde, 1941), and of the total flash (Oh, 1969) are shown for comparison.

The curve in Fig. 12 labeled "Oetzel-Pierce (1969)" is visually fitted to the data points to approximate Oetzel's observation that the

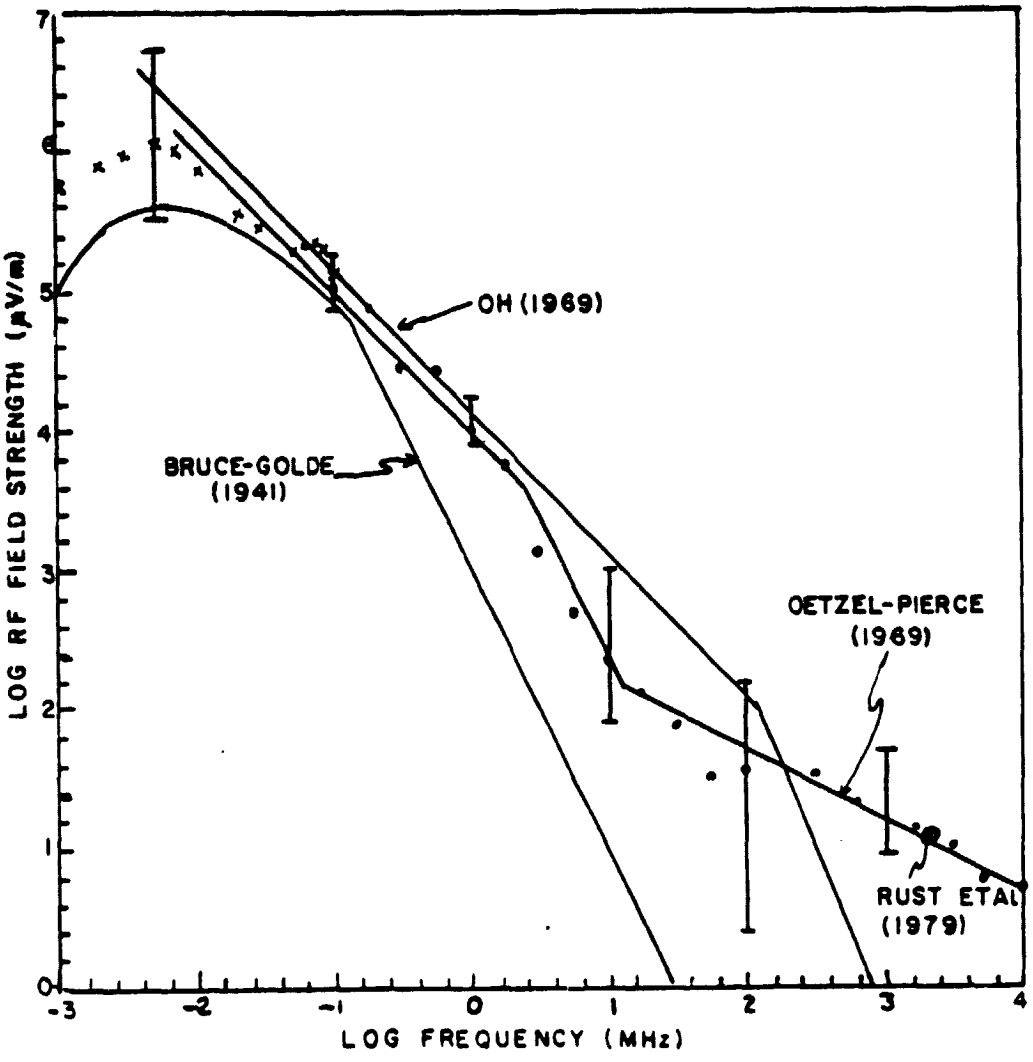


Fig. 12. Composite experimental lightning amplitude spectrum for 1 kHz to 10 GHz, normalized to 10-km distance and 1-kHz bandwidth, derived from diverse data presented by Oetzel and Pierce (1969). Curves are as labeled, and circled x is recent data point by Rust et al (1979).

spectrum goes as 1/f in the lower range, transitions to a $1/f^2$ dependence in the middle range and finally flattens out to a $1/f^{\frac{1}{2}}$ slope somewhere above 10 MHz. It has been known for some time that the return stroke spectrum alone fails to satisfactorily account for radiation on frequencies above a few MHz. Consideration of the total flash gives somewhat better results in this range, but even the Oh (1969) spectrum seems inadequate above a few hundred MHz. Until a reasonable theory taking into account all processes in the lightning discharge is developed, it seems prudent to utilize the experimentally determined spectrum, that is, the Oetzel-Pierce curve of Fig. 12.

## 2.5 Lightning Statistics

In designing a system to detect a lightning flash from space, a potential source of interference to consider is other flashes of lightning taking place at nearly the same time within the instrument's field of view. The statistics of lightning (e.g., flashing rates, time separation, geographic distribution) are therefore important in establishing the resolution requirement of the system.

The geographic distribution of thunderstorm activity has been established on the basis of aural reports from world-wide participating weather stations. It is deficient in several respects; firstly, since the statistic is "days with thunder heard" there is no measure of how many flashes may have taken place, and secondly the data, being gathered by mostly ground stations, gives inadequate coverage for ocean areas. Also, since the aural signal limits detection to about 25-km range, a

significant number of storms occurring between observing stations might be missed. However, the data should be sufficiently precise for planning purposes.

The global distribution of the average annual number of thunderstorm days according to the World Meteorological Organization, is illustrated in Fig. 13. Israël (1973) gives similar distributions for 4-year seasons (e.g., March-April-May). The annual mean number for the United States as determined by the U.S. Weather Bureau (Baldwin, 1973) is shown in Fig. 14. Comparison of the latter map with the same area in Fig. 13 reveals striking discrepancies. Over Florida, for example, Baldwin's map shows a maximum of 100 days, while Israël records only 60.

C.E.P. Brooks' version of the number of cloud-to-ground strokes per square mile per annum is reproduced in Fig. 15. This map represents only flashes to flat terrain, and was derived from observations of 1,950 events combined with data on thunderstorm days, with allowance for the variations in the ratio of intracloud and cloud-to-ground flashes. A different version of the distribution of the total number of discharges per $km^2$ per year is shown in Fig. 16. This distribution was obtained by Kolokolov (1968), who used data from a network of flash counters in the Soviet Union recording storm durations and number of discharges to determine a relationship between the annual number of thunderstorm days and the number of discharges per $km^2$. On a monthly basis, Pierce (1968) has found that the monthly flash rate ($F_m$, in $km^{-2}$) is related to the monthly number of thunderstorm days ($D_m$) by:

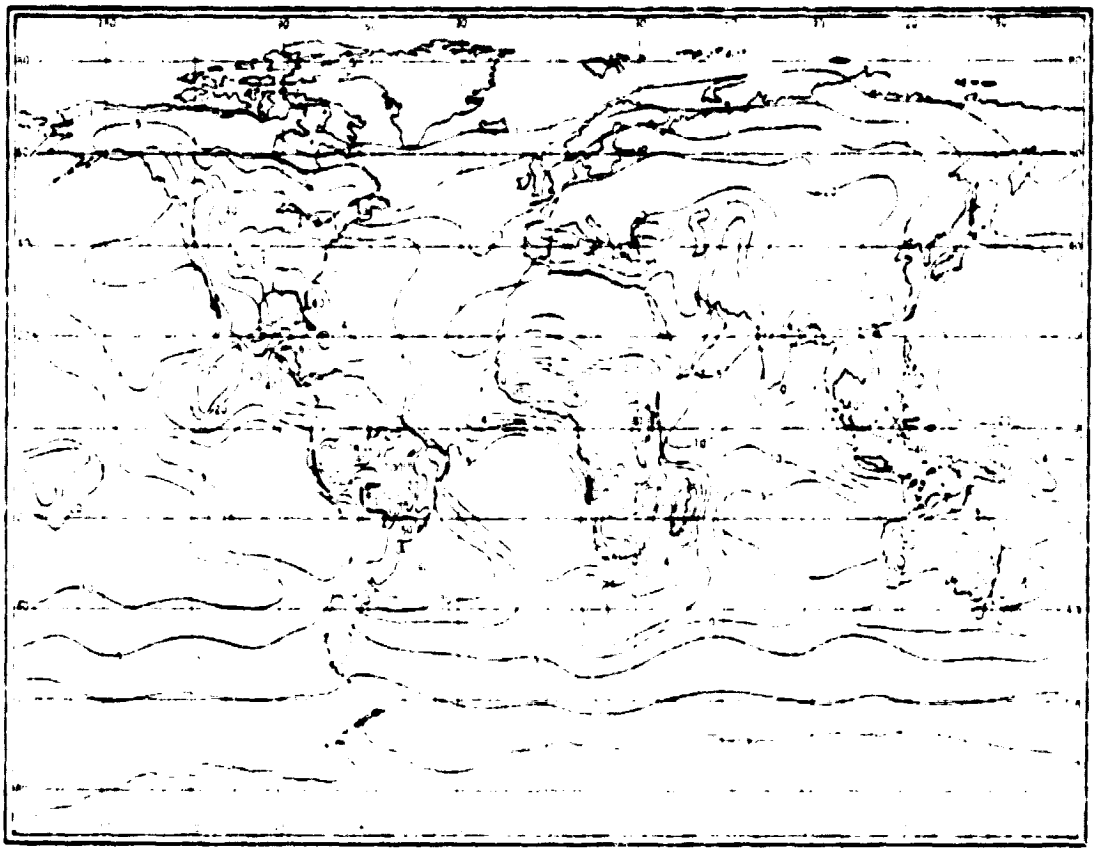

Fig. 13. Global distribution of mean annual number of thunderstorm days (c.f., Hart and Malone, 1979).

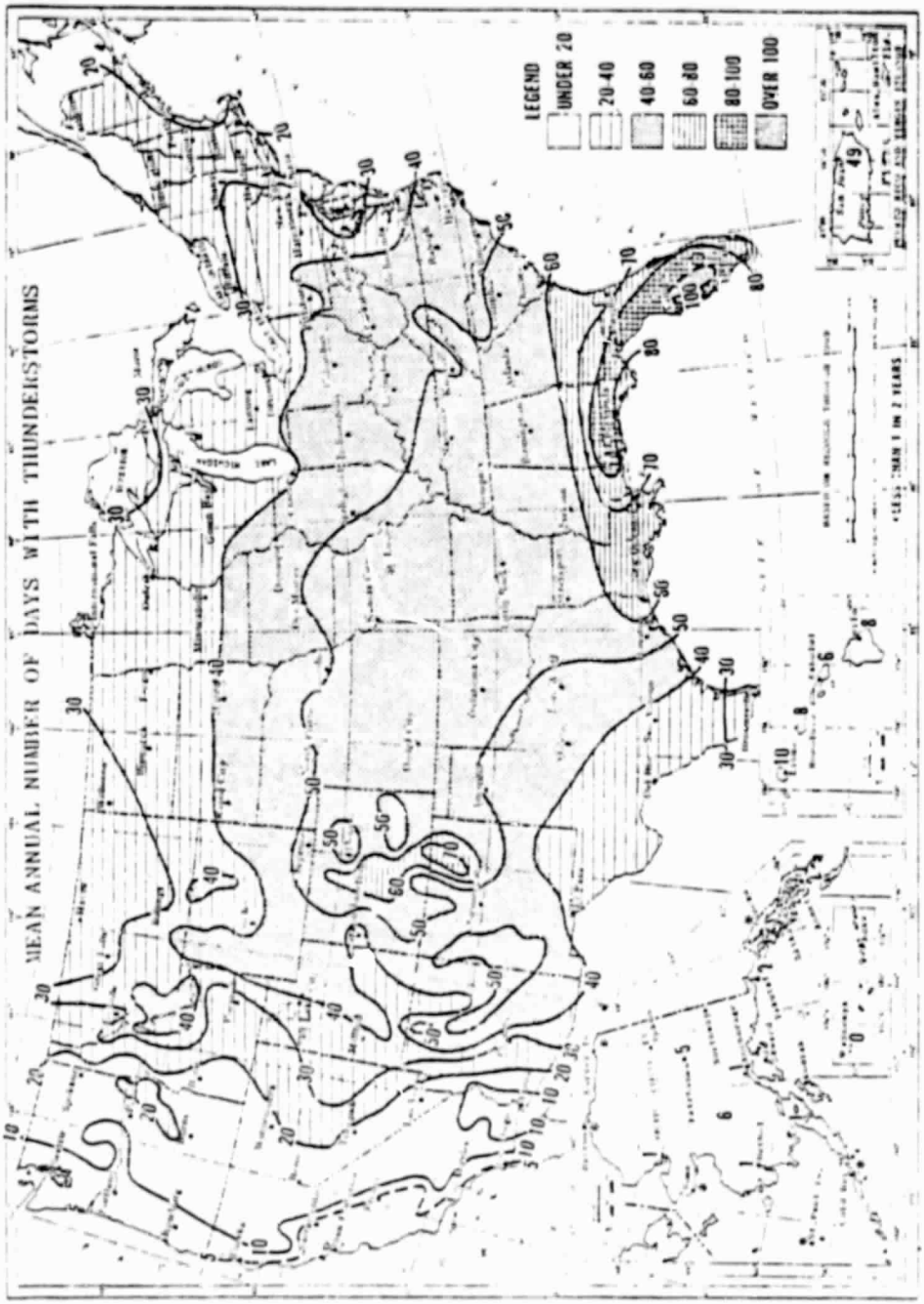


Fig. 14. Mean annual number of days with thunderstorms in the United States (Baldwin, 1973).

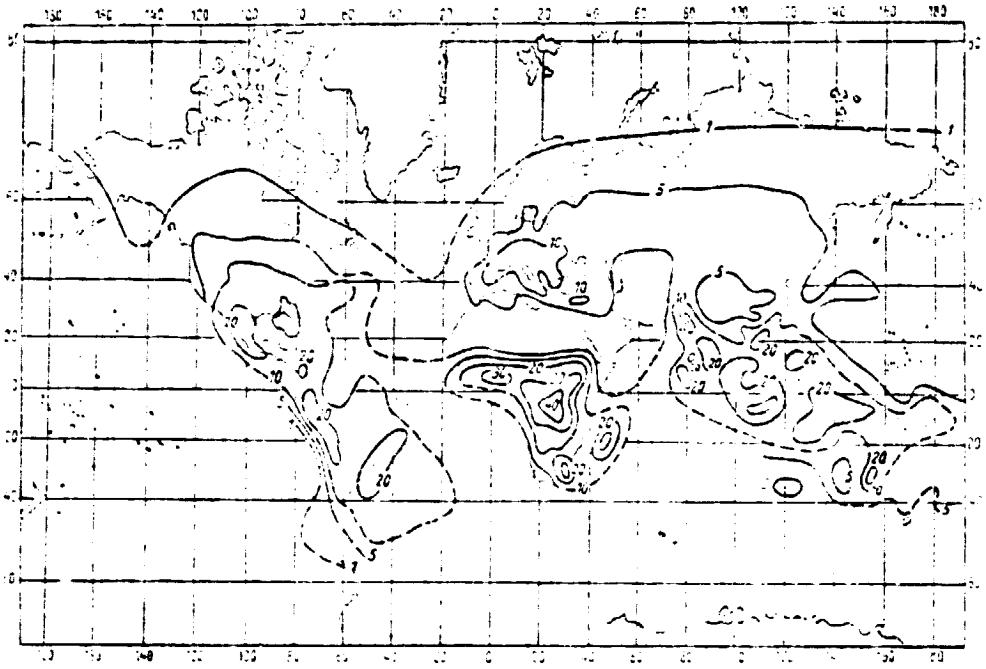

Fig. 15. Global distribution of the mean annual number of lightning strokes to ground. Contours designate number of strokes per square mile (multiply by 0.39 to obtain number per square kilometer). (Israël, 1973).

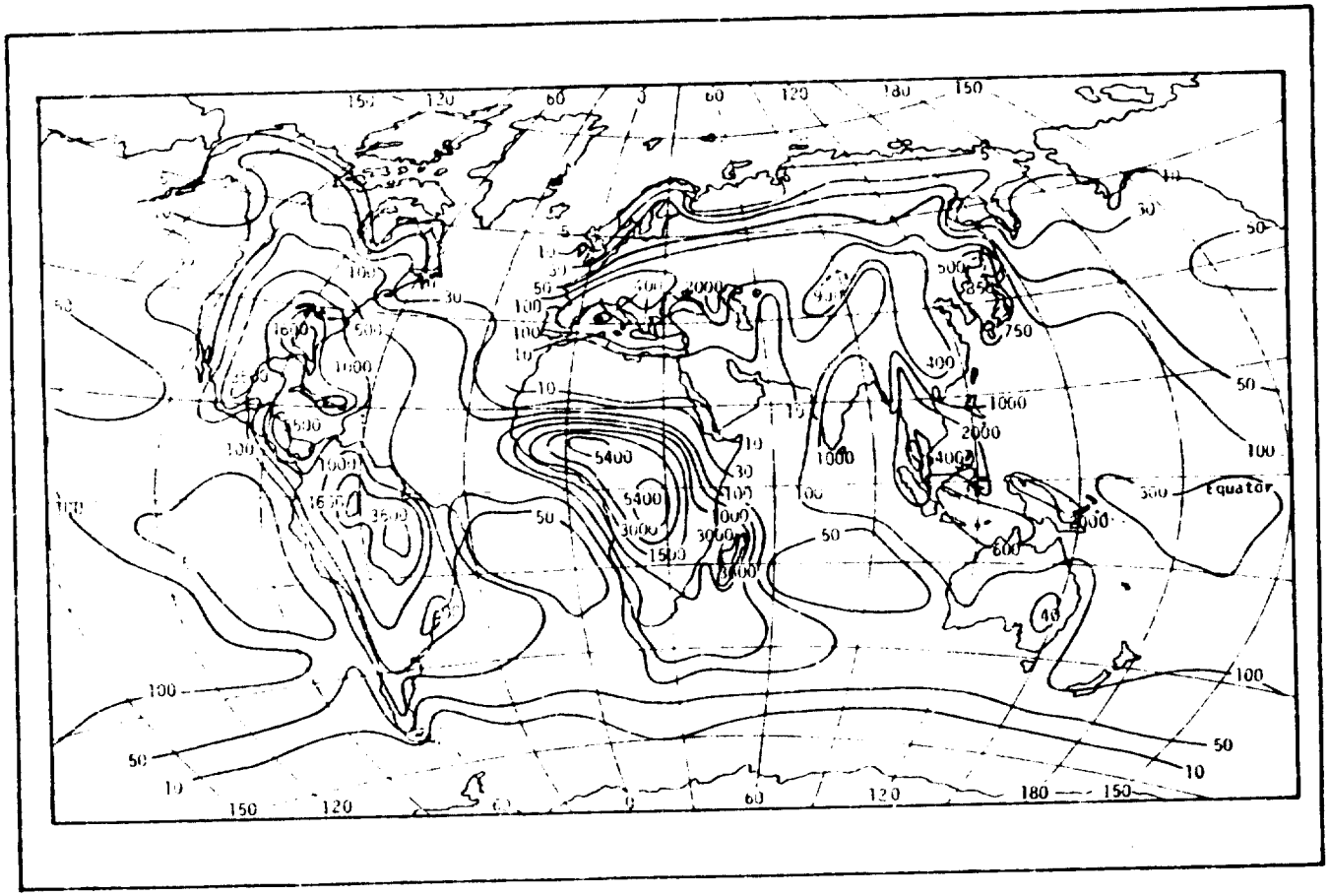


Fig. 16. Global distribution of number of lightning discharges per annum as derived by Kolokolov (see Hart and Malone, 1979).

$$F_m^2 = aD_m + a^2D_m^4$$

where the constant $a = 3(10^{-2})$. However, a recent comparison of flash counter data and meteorological reports of thunderstorm days by Lundquist (1980) in Sweden shows that a significant number of flashes must be recorded (independently on a flash counter) before a meteorologist will classify the day as a thunderstorm day based on his own visual and aural assessment (see Table 1).

Table 1. Thunderstorm days and lightning counter recordings in Sweden (Lundquist, 1980).

| Number of counts in one day at the weather station | Probability (%) that this day has been designated a thunderstorm day by the station |
|---|---|
| 1-2 | 8 |
| 3-5 | 32 |
| 6-10 | 53 |
| 11-20 | 61 |
| 21-40 | 69 |
| 41-80 | 88 |
| 81-160 | 89 |
| over 160 | 95 |

Horner (1965) has utilized the results of several reported methods for counting flashes to estimate that about $1.5(10^{-5})$ flashes per $km^2$ per sec ($km^{-2}s^{-1}$) take place in equatorial regions at the time of maximum thunderstorm activity. But this amounts to only about 475 flashes $km^{-2}yr^{-1}$, roughly a factor of 10 lower than the maxima found in the equatorial land masses in Fig. 16. Other estimates (e.g., Hart and

Malone, 1979) place the flashing rate at $10^{-4}$ $km^{-2}s^{-1}$, which is comparable to the results of Fig. 16 in the maximum activity regions.

In an individual thunderstorm the flash rate varies from less than one per minute to upwards of ten per minute, with an average over the life of the storm of about 3 per minute or one every 20 seconds. The mean area of a well-developed thunderstorm cell is about 500 $km^2$, so that the flashing rate is again approximately $10^{-4}$ $km^{-2}s^{-1}$. It appears that Horner's (1965) estimate was too conservative by a factor of 10, but this merely points up the dire need for additional measurements with standardized equipment over large geographic areas.

## 3. SOME GEOMETRICAL CONSIDERATIONS

For the conversion of the source function characteristics (section 2) to the situation at satellite heights, it is helpful to consider the geometry involved. The geometry is simple and perhaps obvious, but it leads to interesting consequences.

To illustrate the points of interest for the geosynchronous case, it is sufficient to consider the simplest geometry as sketched in Fig. 17. The pertinent parameters are the look angle labeled "a" at the satellite, the elevation angle "e" at the lightning flash point P, and the ground range R from the flash to the subsatellite point at S. The satellite height H, is taken to be 35,900 km for the geosynchronous case, and the Earth's radius A, is 6371 km. These parameters are related by the expressions:

$$R = Ab \tag{1}$$

$$R = A\left(90 - e - \sin^{-1}\left(\frac{A\cos(e)}{A + H}\right)\right) \tag{2}$$

where the angle "b", expressed in radians, is the angle between the lightning flash and the subsatellite point.

In terms of b, the total area on the surface of the Earth subtended by the solid angle around "a" at the satellite is

$$\text{Area} = 2A^2(1 - \cos(b)) \tag{3}$$

Here, note that $b = 90 - e - a$, where $a = \sin^{-1}\left(\frac{A\cos(e)}{A + H}\right)$.

The line of sight distance to the satellite horizon at "m" is L

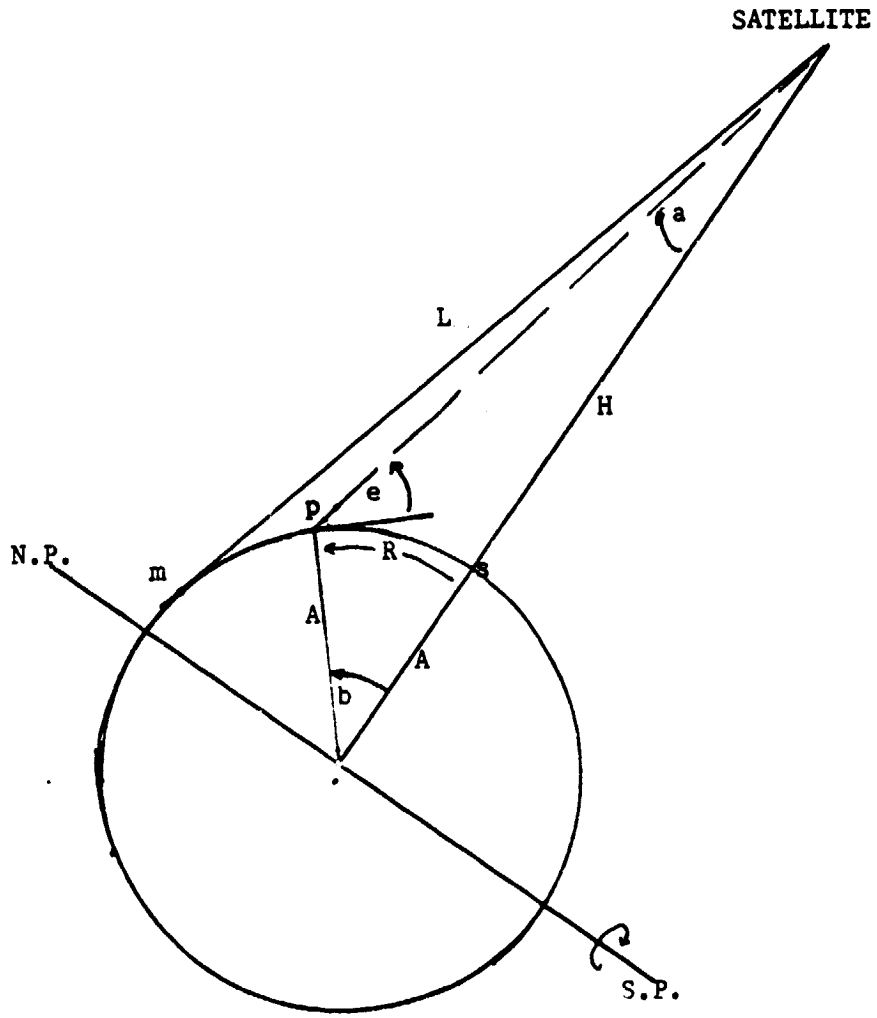


Fig. 17. Geometry of geosynchronous satellite with rf lightning sensor. (Not to scale.)

(Fig. 17), which is 42,748 km for a geosynchronous satellite. If the radio emission were uniform over the surface the "limb darkening" would be approximately 1.5 dB from the subsatellite point to the satellite horizon.

The total coverage given by a geosynchronous satellite located over the equator at 100 $^{o}$W longitude is given in Fig. 18 within the circle for $0^{o}$ elevation. The ground range to the satellite horizon where $e = 0^{o}$ is 9044 km, and the area of the field of view (from eq. 3) is $6.9(10^{7})$ km$^{2}$. The elevation angle, of course, increases toward the subsatellite point to a maximum of $90^{o}$; the loci for $30^{o}$ and $60^{o}$ elevation angles are also drawn in Fig. 18. Here it can be seen that the elevation angles for ray paths to the satellite from lightning flashes in the United States all fall within the range of $30^{o}$ to $60^{o}$. Unless the radiation pattern from lightning discharges is isotropic, this variation in elevation angle will impose an amplitude variation in the signatures received by the satellite from lightning in different places. It is therefore important to determine radiation patterns of lightning by ground-based or airborne measurements.

Now, while the elevation angle is varying from $90^{o}$ at the subsatellite point to $0^{o}$ at the horizon, the look angle a (Fig. 17) goes from $0^{o}$ to only $8.67^{o}$. The resolution of an rf lightning sensor system with a fixed antenna beamwidth would vary considerably over the total field of view of the satellite itself. That is to say, a $1^{o}$-beamwidth antenna looking straight down would cover an area of the Earth's surface of $3.1(10^{5})$ km$^{2}$, but with the antenna boresight looking toward $a = 8^{o}$,

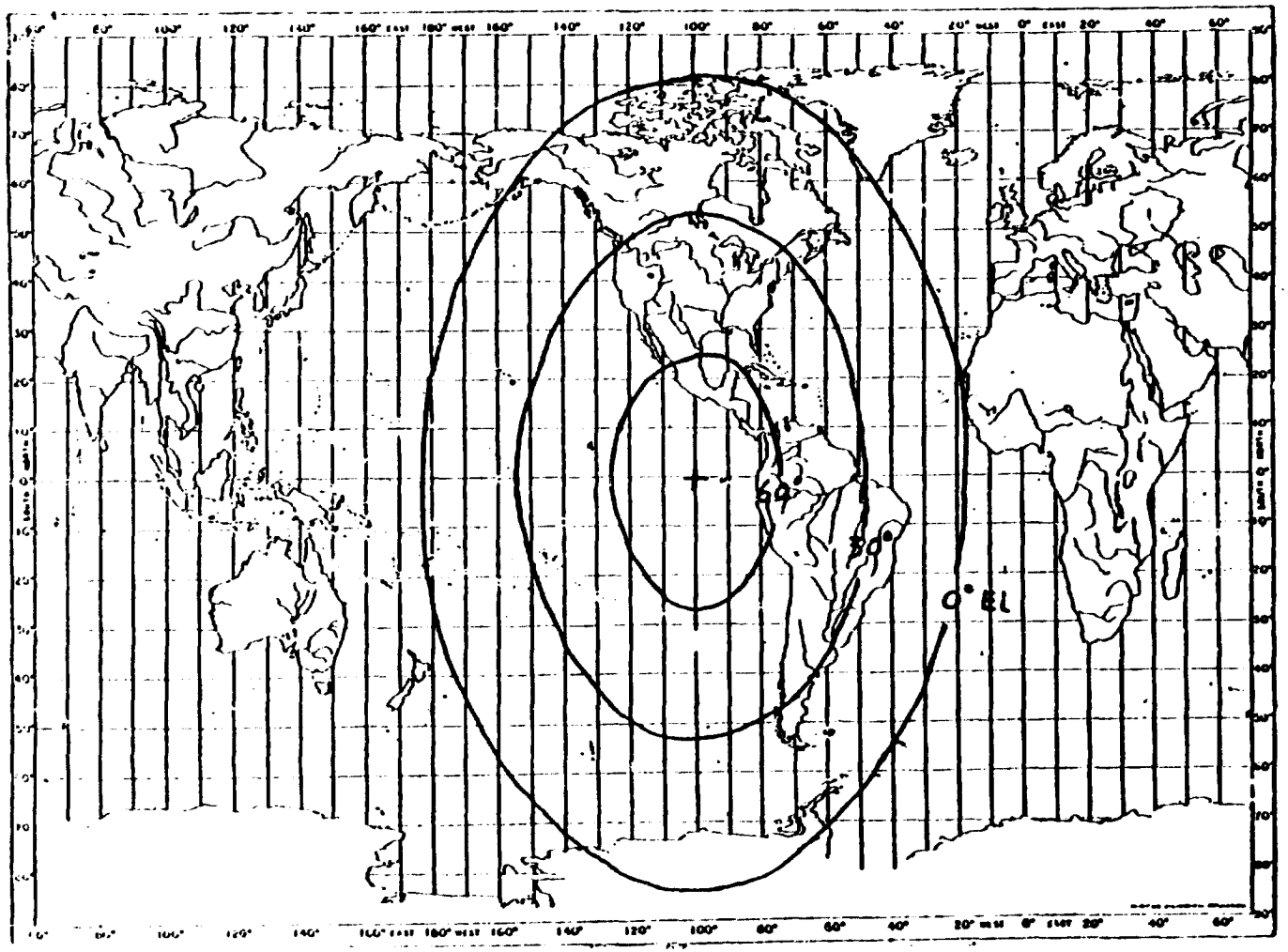


Fig. 18. Field of view as a function of elevation angle for a geosynchronous satellite located over the equator at 100 °W longitude (modified cylindrical projection).

where the elevation angle for the flash would be $22.5^{o}$, the area subtended by the beam would be approximately $3.1(10^{6})$ $km^{2}$, or ten times as large. With presently achievable antenna beamwidths, even at UHF for mounting on satellites, it appears that rf techniques will give poor resolution for lightning location from space, unless more sophisticated direction finding methods such as interferometry (e.g., Warwick et al, 1979) can be utilized.

## 4.0 IONOSPHERIC EFFECTS

An rf lightning signal propagating from the ground to near space will be modified as it passes through the ionosphere in several ways (see Fig. 1). Curtailment of the program precludes a complete study based on the elements of Fig. 1, so assessment of the effects of the effects of ionospheric shielding, absorption, refraction, dispersion and scintillation is given in this section.

### 4.1 Ionospheric Shielding; the Iris Effect

For observations in the HF band, the presence of the ionosphere complicates the geometry discussed in section 3 to a certain extent. Neglecting refraction and assuming a flat Earth the ground range R observable by a satellite at height $H_s$ is approximately (e.g., Horner and Bent, 1969):

$$\left(\frac{R}{H_s}\right)^2 = \left(\frac{f}{f_c}\right)^2 - 1 \qquad (4)$$

where f is the observing radio frequency and $f_c$ is the critical, or penetration frequency of the ionosphere. Inclusion of refraction would in all cases increase the apparent size of the iris. The relationship in (4) becomes inaccurate at large distances from the subsatellite point, and requires modification for a curved Earth, curved ionosphere. It also requires inclusion of the height $H_i$ of the reflecting layer; that is (Herman et al, 1973):

$$\left(\frac{f}{f_c}\right)^2 = 1 - A^2\left[\frac{A + H_s}{A + H_i}\right]^2\left[\frac{\sin^2(R/A)}{A^2 + (A + H_s)^2 - 2A(A + H_s)\cos(R/A)}\right] \quad (5)$$

Using this expression with $H_i$ = 300 km and satellite altitudes of 1500, 6000, and 35900 km, the range as a function of $f_c/f$ is as shown in Fig. 19. Each curve terminates at the satellite horizon. With a constant ionosphere (i.e., no horizontal gradients in electron density), the depicted range can be thought of as the radius of an ionospheric iris which expands or contracts as the ratio $f_c/f$ changes. At a constant ratio, the iris gets bigger with increasing satellite height. Also, for a given satellite height and constant observing frequency the iris expands with decreasing critical frequency; for example, the iris would be larger at night than during daytime due to the more dense ionosphere and higher critical frequency in the latter period. Finally, it is evident that with a fixed ionosphere the iris expands with increasing observing frequency.

With a real ionosphere the iris is not exactly circular due to variations in critical frequency with local time (i.e., longitude) and with latitude. Three examples of the iris distortion, viewed from the vantage point of the Moon, are illustrated in Figs. 20, 21, and 22. In Fig. 20, the Moon transits Greenwich at about 1800UT, so we are looking at the evening side of the Earth. The cross designates the sublunar point for 0800UT. The iris is actually displaced from the sublunar (subsatellite) point for 0800UT because the critical frequency is

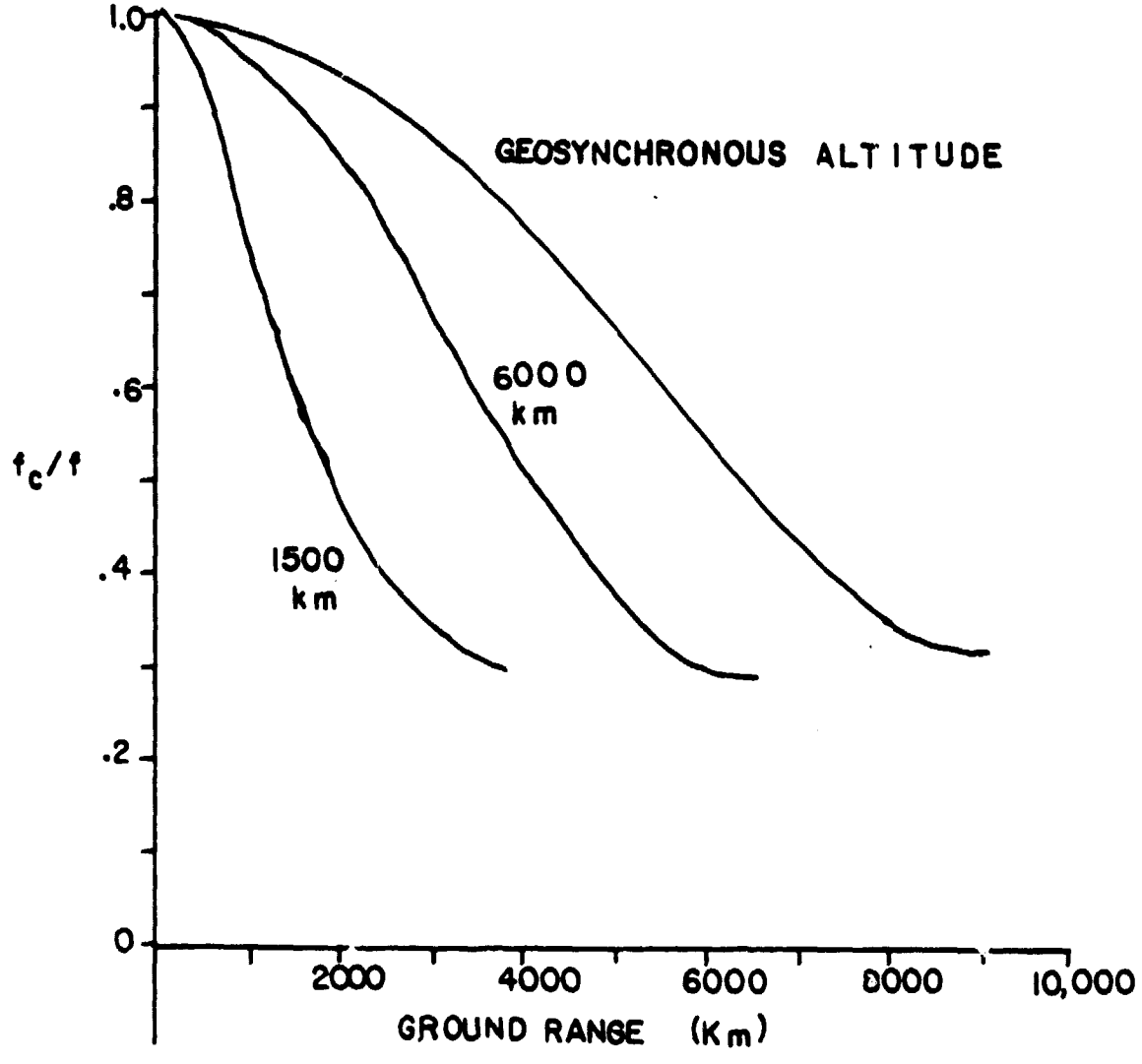


Fig. 19. Distance from subsatellite point to ionospheric cutoff point as a function of the ratio of critical frequency ($f_c$) to observing frequency (f).

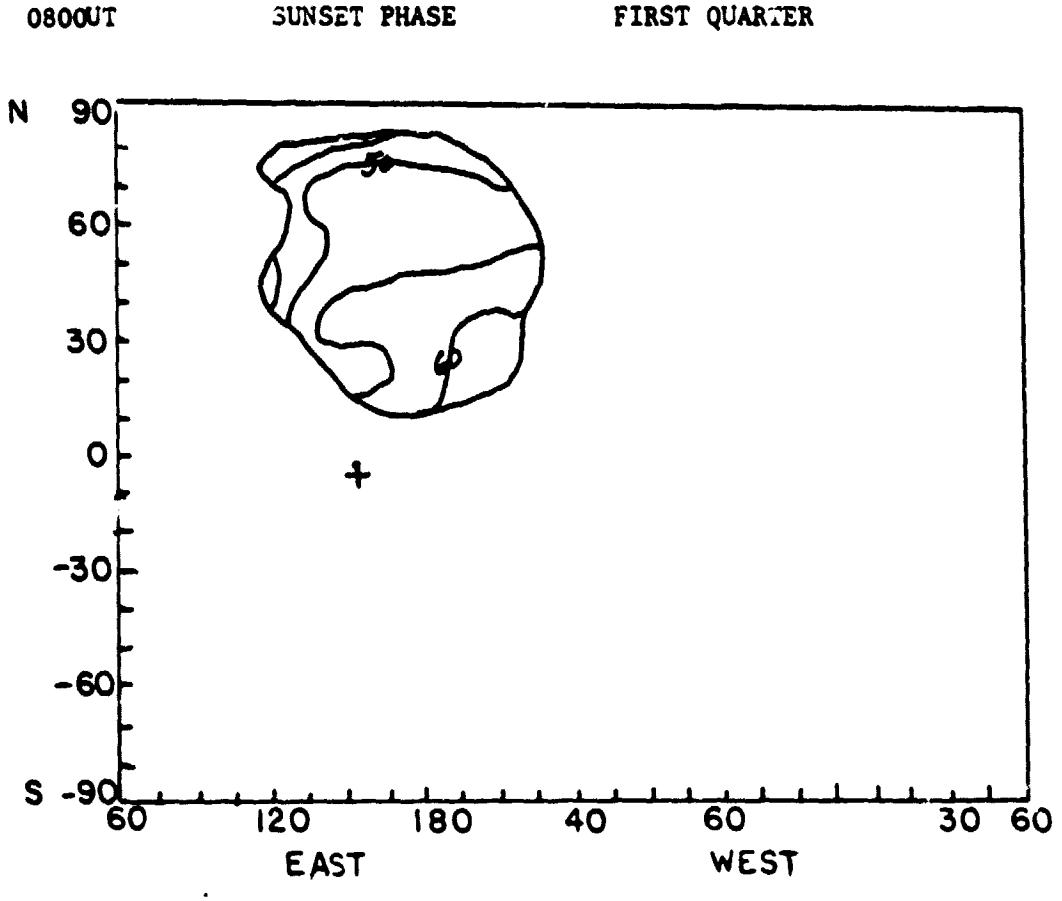


Fig. 20. Ionospheric iris for 9.2 MHz as viewed from the Moon during 1st Quarter (Dec. 3, 1973). The contours are surface atmospheric radio noise power on 1 MHz in dB above $kT_o b$ visible through the iris (Herman, 1974).

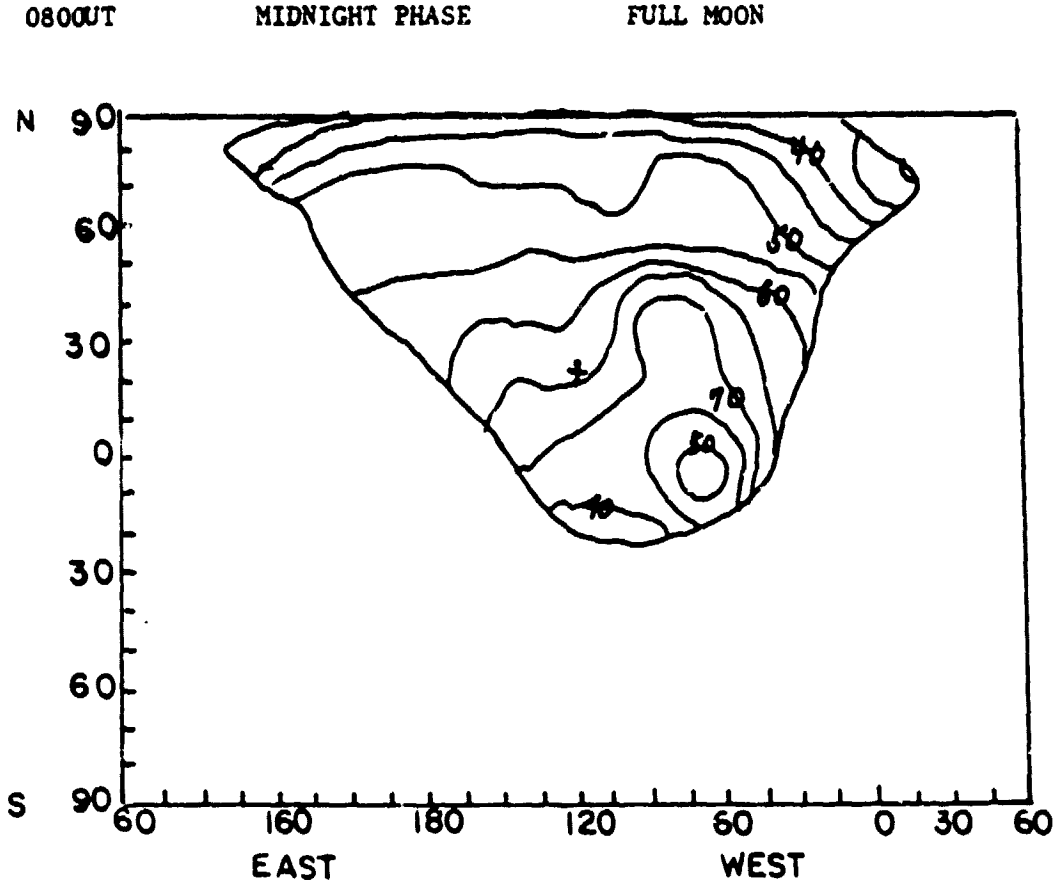


Fig. 21. Same as Fig. 20 but for Full Moon phase Dec. 10, 1973.

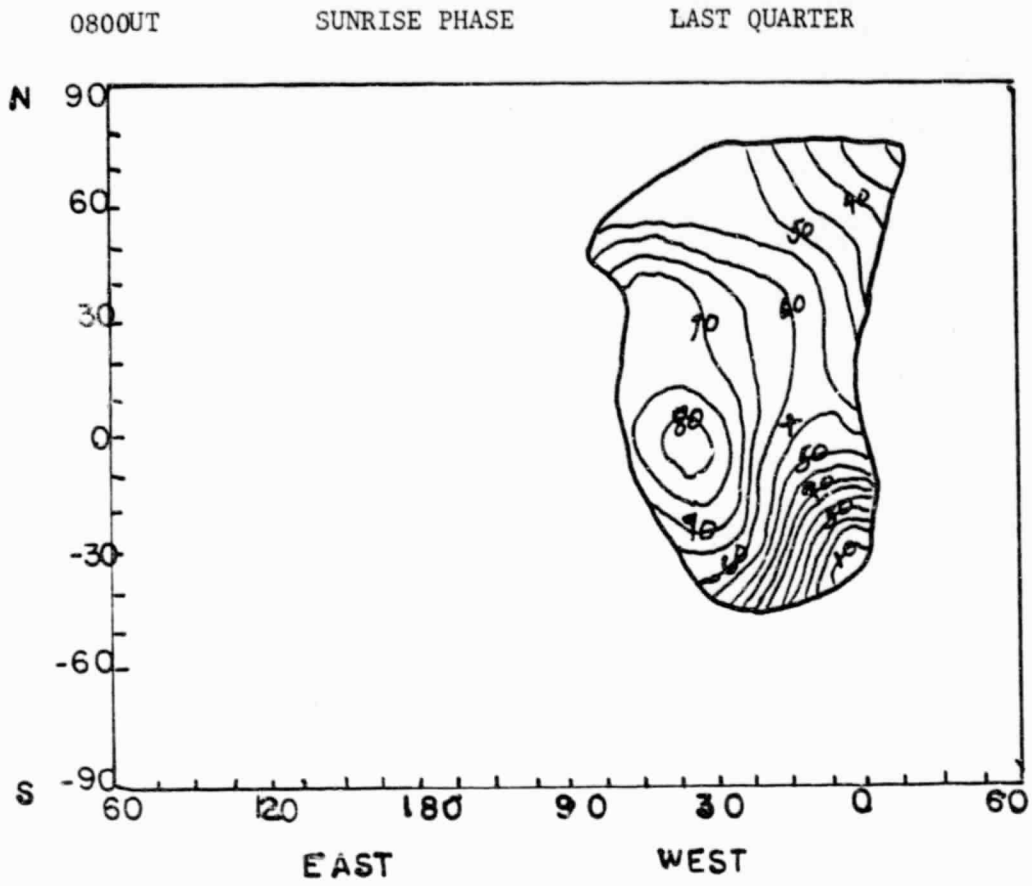


Fig. 22. Same as Fig. 20 but for 4th Quarter phase Dec. 19, 1973.

greater than the observing frequency of 9.2 MHz directly beneath the satellite and it decreases going toward the winter pole. During the course of a 24-hr day this iris would remain approximately constant (for about 3 days centered on 1st Quarter day) while the Earth rotated beneath it. As the Moon progresses along its orbit, however, the picture changes. A week later, for example (Fig. 21), the Moon is full, transiting Greenwich at 2400UT, so our view now is of the midnight side. Note here the much larger viewing area (iris size) for 9.2 MHz compared to that in Fig. 20. Here also, the sublunar latitude has moved northward to its maximum excursion, so the ionosphere has opened up all the way to the north polar region.

Now, as the Moon wanes to 4th Quarter (Greenwich transit about 0600UT), the lunar observer views the sunrise side of the Earth (Fig. 22), and the iris has shrunk, especially toward the east where the Sun has already risen and the critical frequency has increased to daytime values. The latitude of the sublunar point has also swung back to $0^{\circ}$, making the winter pole inaccessible. Finally, when the Moon transits Greenwich at 1200UT (New Moon) it is on the dayside centered at local noon. Here the critical frequency or its appropriate oblique equivalent is everywhere within the satellite horizon greater than 9.2 MHz, so the iris has closed completely (not illustrated). To complete the cycle, about a week after New Moon we would again see the sunset iris (Fig. 20), and with some variation in detail, this would be encountered each lunar month (approx. every 29½ days).

For the geosynchronous satellite case, a similar situation would

exist, except that the observed ionospheric iris would wax and wane over the course of a 24-hr day rather than over a lunar month. Also, the same part of the Earth would always be (more or less) visible to the satellite, in contrast to the opportunity for the Moon-based observer to see the whole Earth as it rotated gradually beneath his relatively fixed ionospheric iris.

In principle it seems as though advantage might be taken of the frequency dependence of the iris geometry to help assess the location of lightning flashes. That is, with a multi-frequency receiver, measurement of the cutoff frequency when the ionospheric critical frequency is known would determine the distance of the flash from the subsatellite point. Such a technique would require detailed knowledge of the status of the ionosphere at the time of measurement. Further, it would have to operate over a limited range of frequencies in the HF band, where unfortunately the spectrum is extremely crowded with deliberate transmissions which at satellite heights would overpower any lightning signatures (see section 5).

## 4.2 Ionospheric Refraction

The principal refractive effect of interest here centers on the error it may introduce in locating the position of a lightning flash by rf direction-finding techniques. That is, the bending of a radiowave ray path in the ionosphere due to refraction will produce a displacement in the arrival angle from the line-of-sight direction (see Fig. 23).

To calculate the ray trajectory through the ionosphere and then

deduce the bending angles $\beta$ and $\beta'$ (Fig. 23), is in general a complicated ray-tracing problem. To demonstrate the output of such a process, a sample ray tracing result for a ray path from a 20-MHz transmitter on a satellite well above the electron density peak of the ionosphere to a receiver at Boulder, Colorado is shown in Fig. 24. Reciprocity would hold in this case, so the arrival angle for a lightning flash at Boulder would be displaced by about $3^{\circ}$ from the line of sight direction. It is emphasized that this is only an illustrative example; the arrival angle error would be different for ionospheric conditions different from those used in the ray-trace calculations and for a different frequency.

A simple approximation due to D.K. Bailey (see Lawrence et al, 1964) allows calculation of the total bending $\tau = \beta + \beta'$ assuming no magnetic field and a spherically stratified ionosphere in which the electron density profile is parabolic. That is:

$$\tau = \frac{d + d'}{3A} \left(\frac{f_c}{f}\right)^2 \left(1 + \frac{H_i}{A}\right)\left(\cos^2 a + \frac{2H_i}{A}\right)^{-3/2} \sin(a) \qquad (6)$$

Here, d and d' are the lower and upper half thicknesses (not necessarily equal) of the parabolic layer centered at the height of maximum electron density (also called the reflection height) $H_i$, and a is the apparent zenith angle (complement of the elevation angle) at the ground.

Applying this equation to the conditions of the example in Fig. 24 (i.e., $f_c$ = 9 MHz; f = 20 MHz; a = $66^{\circ}$; $H_i$ = 382 km) with $\tau$ = 153 milliradians (= $5.76^{\circ} + 3.03^{\circ} = 8.69^{\circ}$), then d + d' is 2287 km. The formula

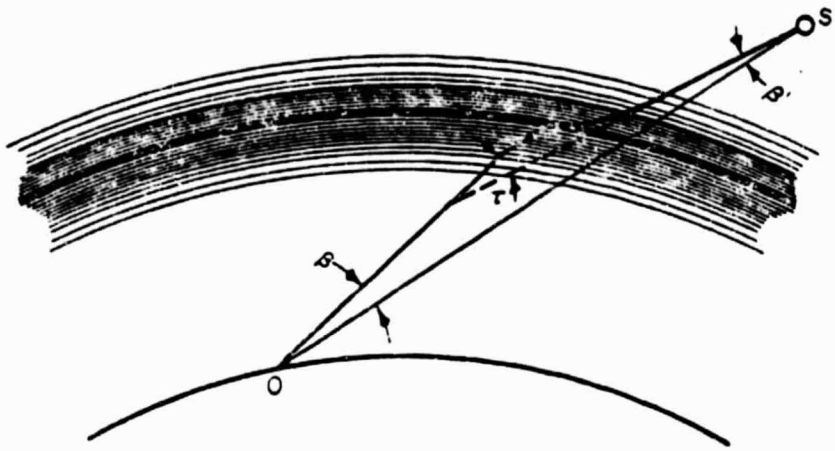


Fig. 23. Refractive bending of a ray path through a spherically stratified ionosphere (Lawrence et al, 1964). Not to scale.

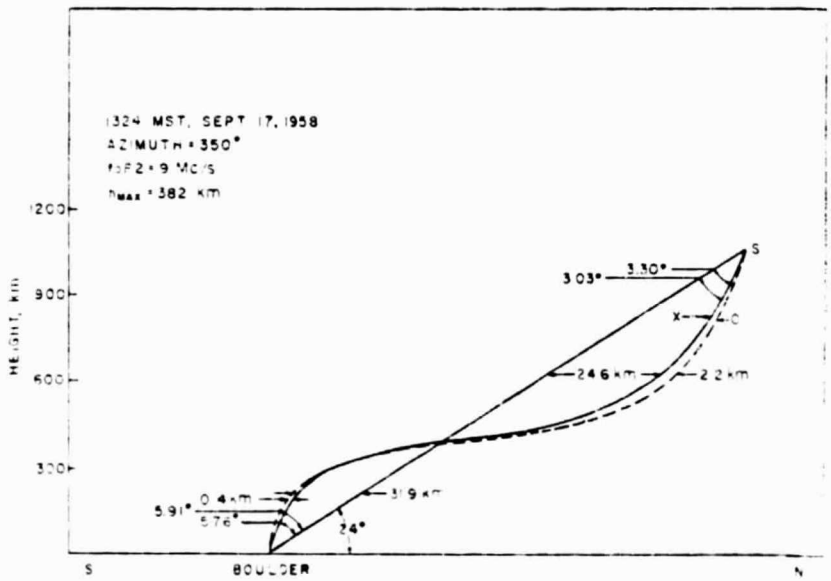


Fig. 24. A calculated 20-MHz ray path from a satellite (s) at an elevation angle of 24° in the northern sky to Boulder, Colorado (Lawrence et al, 1964).

is only an approximation, of course, and according to Lawrence et al (1964) it should not be used for frequencies which are less than about twice the oblique critical frequency for a given value of zenith angle (a). In any case, the total bending decreases with the square of the observing frequency, and with increasing angle of incidence (i.e, decreasing zenith angle). Also, the thicker the ionosphere the greater the angular error, as expected.

Other ray-tracing calculations (Carru et al, 1960) have shown that with the satellite at altitudes above about 2500 km the angular error measured at the ground ($\beta$) remains approximately constant with a further increase in altitude, but does continue to decrease as the elevation angle increases. Their results for 20 MHz propagating to a satellite above 2500 km through an ionosphere with $f_c$ = 12.7 MHz shows the following relationship:

| | | | | | |
|---|---|---|---|---|---|
| Elevation Angle (deg.): | 38.4 | 41.3 | 44.2 | 55.6 | 61.4 |
| Angular Error (deg.): | 9.5 | 6.9 | 5.1 | 3.6 | 1.8 |

It is expected that the angular error at the satellite would be smaller than this. Additional ray tracing work would be required to obtain quantitative estimates for other operating frequencies and ionospheric conditions, but in general, the error would be smaller at higher frequencies, and would be smaller for lower ionospheric electron densities.

## 4.3 Ionospheric Absorption

Dissipative attenuation, better known as "absorption" of a radiowave in the ionosphere takes place due to collisions between free electrons and neutral gas molecules, which converts part of the rf energy into heat. If the propagation direction is not perpindicular to the magnetic field, the absorption per unit path length can be approximated by (e.g., Davies, 1965):

$$k = \frac{e^2}{2\epsilon_o mc} \frac{1}{u} \frac{N\nu}{(\omega \pm \omega_L)^2 + \nu^2} \qquad (7)$$

where e and m are the electron charge and mass, c is speed of light, $\epsilon_o$ is permittivity of free space, u is the ionospheric refractive index, N is the electron density, $\nu$ is the collision frequency between electrons and neutrals, $\omega$ ($=2\pi f$) is the angular wave frequency, and $\omega_L$ is the longitudinal component of the angular gyrofrequency. With the equation in MKS units, k is in nepers per meter, where 1 neper = 8.69 dB. To get the total absorption along the path from lightning flash to receiver, this equation must be integrated because both N and $\nu$ are height dependent. That is, the absorption L, in dB, is $L = -8.7 \int k ds$, where ds is an elemental unit of length along the ray path. (L is negative because absorption is a loss term.)

In the lower ionospheric D region ( 60-90 km) the refractive index remains near unity because of the relatively low concentration of electrons, and the absorption is then governed mainly by the product of N and $\nu$ . This absorption, usually referred to as "non-deviative",

becomes approximately proportional to the inverse square of the wave frequency when $\omega^2 >> \nu^2$ and $\omega^2 >> \omega_L^2$. In middle latitudes we find $f_L$ ($= \omega_L/2\pi$) is about 1.5 MHz, while $\nu$ varies roughly from $10^7$ $s^{-1}$ at 65 km to $10^5$ $s^{-1}$ at 95 km (Little et al, 1956).

The large variability in electron density, however, has the greatest effect on the non-deviative absorption magnitude. Due to this, the absorption varies diurnally (with maximum near local noon), seasonally (with maximum in winter), and with the solar cycle (maximum in solar maximum years). At night the D region electron population is normally very small, and non-deviative absorption is much reduced.

The plus and minus signs on the gyrofrequency in eq. 7 show up because the ionosphere is a birefringent medium for radiowaves, and refer to the ordinary and extraordinary components of the wave, respectively. Thus the absorption is greater for the extraordinary component. At 30 MHz, for example, the amount of absorption (in dB) of the extraordinary wave is approximately 20% greater than that for the ordinary wave.

A different situation exists when the radiowave frequency f is very close to the critical frequency $f_c$. At the reflection level where $f = f_c$, the refractive index goes to zero, and u thus becomes by far the dominant factor in eq. 7. The amount of signal attenuation, in this instance called "deviative" absorption, thus becomes very large near the reflection level. Deviative absorption is not, in general, inversely proportional to frequency squared.

To demonstrate the effects of absorption, let us assume a somewhat

ordinary mid-latitude day, ionospherically speaking, where the maximum F2 layer and E layer critical frequencies are 12 MHz and 3.5 MHz, respectively, and the gyrofrequency is 1.5 MHz. The variation of absorption with ordinary wave frequency for this circumstance is illustrated in Fig. 25. Note the very large deviative absorption contribution near the E- and F-layer critical frequencies, and maximum nondeviative absorption where $f = 1 + f_L$.

## 4.4 Ionospheric Dispersion

The ionosphere is acknowledged as a dispersive medium because the velocity of a radiowave travelling through it varies with frequency. To see this, note that the change in phase path length $\Delta p$ relative to the free space path is:

$$\Delta p = - \frac{1.6(10^3)}{\omega^2} \int N ds \qquad (8)$$

where N is the electron density to be integrated along the path s, and the constant ($=1.6(10^3)$) is in MKS units. The integral of Nds is generally referred to as the total electron content (TEC). The group path length is simply $-\Delta p$, so the group path delay time is $\Delta T = - \Delta p/c$. In other words, in an rf pulse of lightning radiation passing through the ionosphere the lower frequency components travel slower (have a greater delay time) than the higher frequency components. The difference in delay time ($\Delta T$) for two frequencies $f_1$ and $f_2$ is

$$\Delta T = \Delta T_1 - \Delta T_2 \qquad (9)$$

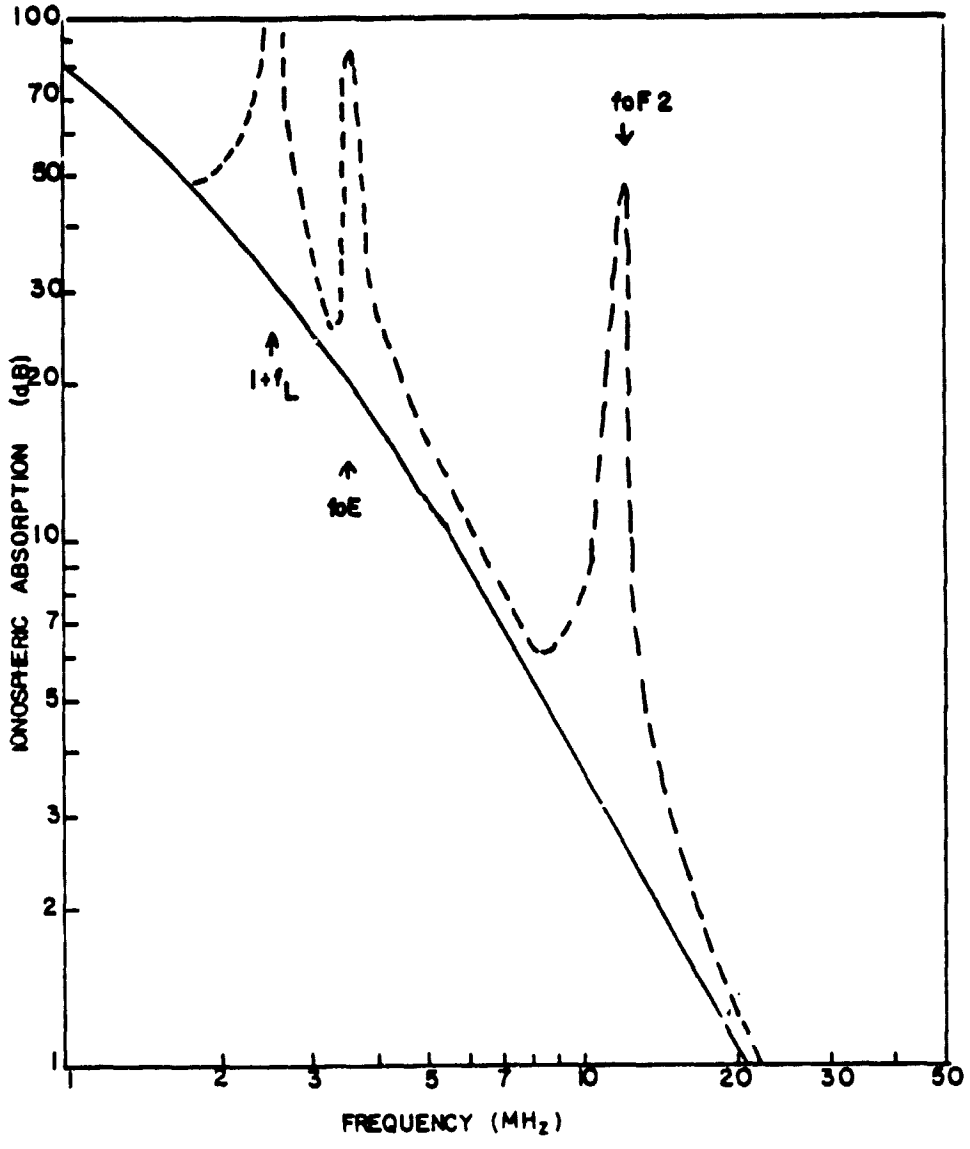


Fig. 25. Ionospheric absorption at noon time in midlatitudes as a function of frequency. Ordinary wave critical frequencies of the E and F2 layers are indicated by foE and foF2. Solid curve is non-deviative; dashed curve is total deviative plus non-deviative.

so that, from eqs. 8 and 9,

$$\Delta T = 1.35(10^{-13}) \frac{f_2^2 - f_1^2}{(f_1 f_2)^2} \sec \phi \int N ds \qquad (10)$$

where $\phi$ is the local zenith angle, and the numerical constant is such that when f is in MHz, $\Delta T$ is in $\mu$sec. Obviously, the greater the frequency separation, the greater is the difference in arrival time of the pulse components until $f_2$ gets very large. An illustration of this variation for two frequencies (27.7 MHz and 42.94 MHz) as a function of TEC and zenith angle ("look angle") is given in Fig. 26. The delay time difference increases with increasing TEC and with increasing zenith angle (i.e., decreasing elevation angle), and with TEC = $10^{18}$ electrons per $m^2$ and $\phi = 60^\circ$, $\Delta T = 205\ \mu$sec. Given $f_1 = 30$ MHz and $f_2 = 300$ MHz under the same conditions, $\Delta T = 297\ \mu$sec, but increasing $f_2$ to 1000 MHz increases $\Delta T$ only to 300 $\mu$sec. As a final example, the arrival time difference between the lightning flash components at 300 MHz and 1000 MHz would be only 2.7 $\mu$sec due to ionospheric dispersion in this case. Any additional apparent dispersion might be attributed to source structure (see section 2.3).

## 4.5 Ionospheric Scintillation

Ground-based observations of radio star and satellite signals have shown that irregularities in the electron density distribution of the ionosphere impose rapid phase and amplitude fluctuations on the propagating radio waves, as well as fluctuations in apparent angular position

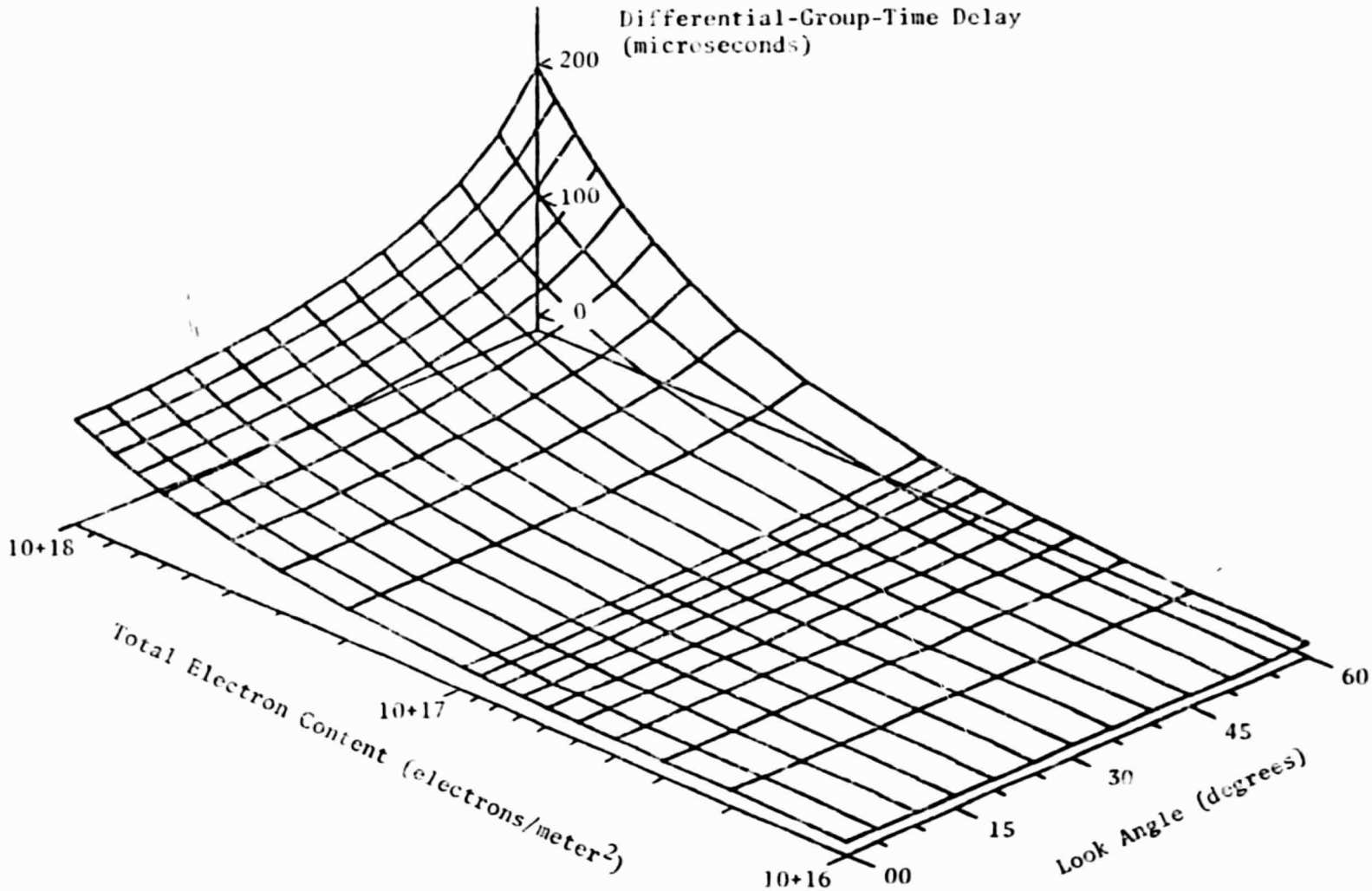


Fig. 26. Differential-group-time delay between 27.70 MHz and 42.94 MHz as a function of total electron content (TEC) and look angle (Chiburis and Jones, 1974).

of the source. The fluctuations are commonly referred to as scintillations, reminiscient of the scintillation of visible stars viewed through the turbulent atmosphere. Because the scintillation effect is frequency dependent, the correlation between simultaneous measurements on spaced frequencies deteriorate as the spacing is increased, and this imposes limitations on the available observing bandwidth. Moreover, since an rf lightning signal is characteristically a short pulse of radiation, the decorrelation in frequency implies that the pulse waveform would also be distorted.

Most models and theories of the scintillation process are based on weak scattering theory, wherein the ionospheric irregularities causing the signal to scatter and scintillate are approximated by a thin diffraction screen positioned near the height of the F-layer peak density (e.g., Goodman, 1975; 1978). Moreover, in most models the signal source (satellite transmitter or radio star) is at a large distance above the ionosphere and the receiver is on the ground, relatively close to the diffraction screen. Theory suggests that as the wave front passes through the screen it first develops phase fluctuations because the screen is moving transverse to the propagation path, and these progress into amplitude fluctuations as the wave propagates further and further away from the screen. Amplitude fading depths of up to 25 dB on 2.2 GHz satellite transmissions received at the ground have been observed (Mullen et al, 1978).

The scattering effect becomes more pronounced with increasing irregularity strength ($\Delta N/N$), mean electron density ($\tilde{N}$), or screen

thickness (Z). The irregularity size determines which wave frequencies are affected, and since a wide spectrum of sizes ranging from 10 m to 10 km and more may be present simultaneously in the ionosphere (Herman, 1966), the scintillation effect can be seen on frequencies from HF to a few GHz received at the ground. Ulazek et al (1975) have investigated the effects on available observing-bandwidth and correlation of spaced frequencies. To demonstrate the results, let us assume a power law spectrum of the irregularity size distribution (Rufenach, 1972) in an ionosphere where the irregularities are weak ($\Delta N/N = 4\%$) and the mean electron density ($\bar{N} = 7(10^5)$ elec/cm$^3$) corresponds to a critical frequency of 7.5 MHz. The coherence bandwidth ($\Delta f/f$) of a 120 MHz signal passing through this ionosphere would be 3.7%, and a 240 MHz signal would have a bandwidth availability of 19.4% under the same conditions. The frequency correlation near 120 MHz would be 0.76, and for 240 MHz it would be 0.96.

The improvement with increasing frequency is a consequence of the inverse frequency dependence of the scintillation effect, which is generally valid. However, near the equator where very small irregularities of a few meters size develop at night, strong scintillation can be observed on GHz frequencies received at the ground (e.g., Taur, 1973).

For a given ionospheric condition and observing frequency, it has been found that the signal from a radio star measured at the ground has a greater scintillation depth than does that from a satellite transmitter. Consideration of the relationship between the Fresnel zone

radius of the irregularities and the scintillation amplitude (Lawrence et al, 1964) reveals that the distance between the signal source and the scattering screen is an important factor. That is, if z' is the distance from the source to the irregularity screen and z is the distance from the ground observer to the screen, then the mean-square scintillation amplitude for the source is a fraction

$$F_s = \left(\frac{z'}{z + z'}\right)^2 \tag{11}$$

of the amplitude if the source were at an infinite distance from the screen.

Thus, in attempting to determine scintillation effects on a signal transmitted from the ground and received by a satellite, one cannot simply assume reciprocity of propagation and apply ground-based measurement results to the problem. In the special case where the irregularity layer is 400 km above the Earth and the satellite is at an altitude of 800 km, the fraction compared to a radio star (approximately infinite) source would be 1/4 whether the satellite were transmitting or receiving (because z = z'). For a geosynchronous satellite in the transmitting mode, z' = 36000 km and z = 400 km so that $F_s$ = 98%. However, if the situation were reversed as in the case where the geosynchronous satellite were observing a lightning flash from the ground, $F_s$ would be only 1.1%. We therefore conclude that scintillation effects will be small on a lightning rf signal propagating from the ground through the ionosphere to a geosynchronous satellite.

## 5.0 THE NOISE AND INTERFERENCE ENVIRONMENT

Once the rf signature has been generated by a lightning flash and has propagated through the ionosphere to the geosynchronous satellite it must be detected and identified. The two major elements to be considered in establishing identification and detectibility are (1) the character of the ionospherically-modified signature and (2) the noise and interference environment within which the signature must be observed. These two elements are addressed below; the modified signature is discussed in section 5.1 and subsequent sections are devoted to a summary of the environment. The discussions here are brief, and can be supplemented by reviews by Herman (1978, 1979) and Haber et al (1976). The final section (5.4) compares the lightning signature with the noise background to establish detectibility.

### 5.1 The Modified RF Spectrum of Lightning

Beginning with the composite spectrum of lightning derived in section 2.4, we apply the ionospheric effects discussed in section 4 to obtain a modified rf amplitude spectrum applicable to observation at geosynchronous height. The result, illustrated in Fig. 27, is only a preliminary working model in that only the effects of ionospheric cutoff, deviative and non-deviative absorption, and inverse distance loss to geosynchronous height have been accounted for. Spectral distortions due to any possible scintillation effects (expected to be small in any event) or bandwidth limitations have been ignored.

Also ignored are any effects due to differential group path delay

as a function of operating frequency. When considering the amplitude spectrum from the total lightning flash, where it is assumed that the time window of observation is sufficiently long to include all rf components of the flash, differences in propagation delay time on different frequencies (section 4.4) are unimportant. However, any scheme for identifying the rf lightning signature through observation of the time structure of the source itself (e.g., section 2.3) would have to take into account the ionospherically imposed differential time delay of the rf pulses on different frequencies.

With regard to the spectrum itself (Fig. 27), the solid curve applies to a daytime observation where the F2-layer critical frequency is 12 MHz and the absorptive attenuation is as depicted in Fig. 25. Maximum field intensity is found on a frequency slightly higher than 12 MHz because of the large amount of deviative absorption right at the critical frequency. The absorption loss then decreases rapidly with frequency, and above about 30 MHz (in this case) it becomes insignificant. The vertical 'bars of variability' indicate the range of variation in the source ratiation strength, and the horizontal bar shows the range of expected variation in effective cutoff frequency. The latter range is from about 4 MHz for a nighttime critical frequency with the radiowave vertically incident upon the ionosphere (elevation angle $90^{o}$) to about 40 MHz for an obliquely incident radiowave passing through a daytime ionosphere in a sunspot maximum year.

The spectrum in Fig. 27 is thought to be representative of what might be the case at geosynchronous altitude. Additional investigation

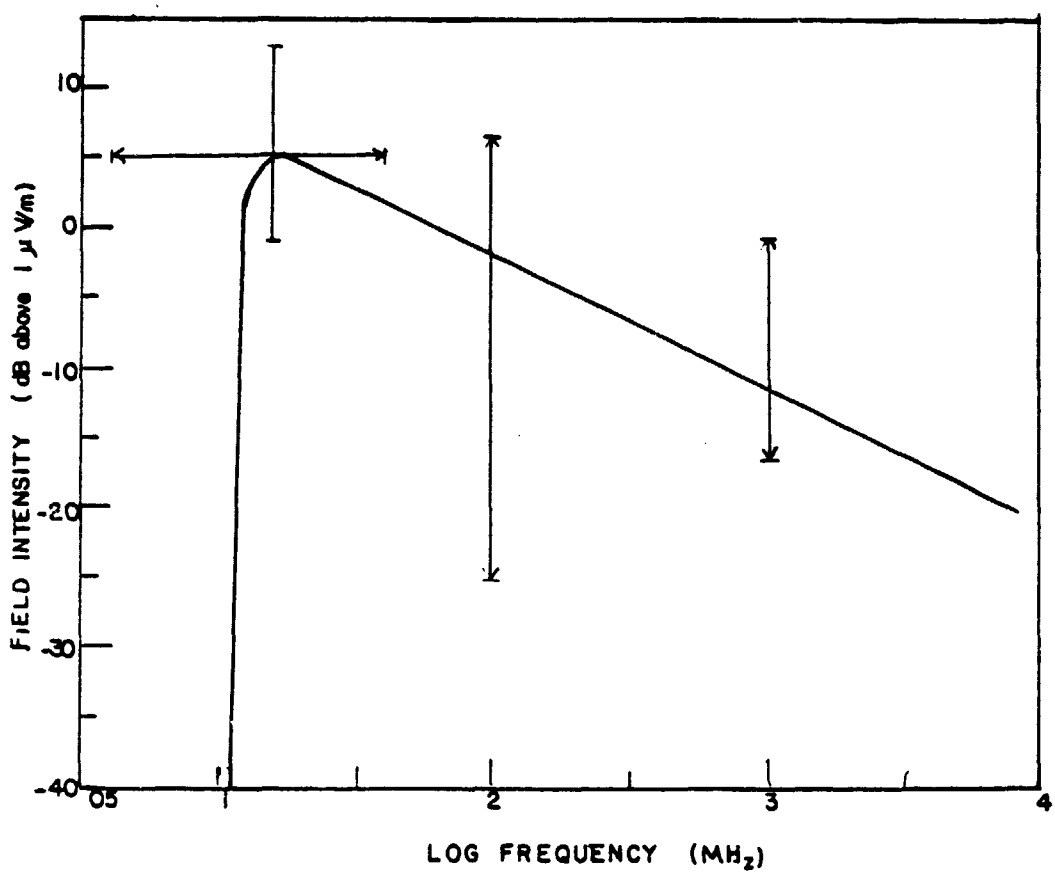


Fig. 27. Radio frequency amplitude spectrum of the peak radiation from lightning expected to be observed from a geosynchronous space platform.

would be required to ascertain the statistical variation in the spectral amplitude, since both the source strength and the propagation losses vary with time and from one event to another. Such information would be very helpful in addressing the question of probability of detection with a given threshold response, including the required characteristics of a satellite-borne rf lightning sensor.

## 5.2 Natural Noise in Near Space

In assessing the noise environment in space it is helpful to separate natural sources from man-made sources, as identified in Fig. 1. In this section natural noise is discussed.

Although the rf radiation from a lightning flash is our desired signal, other lightning flashes within the antenna beam occurring at the same time constitute interfering sources of noise unless the rf sensor has sufficient spatial and temporal resolving power to separate one flash from another. The information given in section 2 suffices for lightning as both the signal source and one of the anticipated natural noise sources. Additional study would be required to determine the detailed effects of this source.

Apart from lightning, probably the most important source of natural noise germane to the present investigation is the galactic, or cosmic noise background. To be sure, intense noise is generated by the magnetosphere on frequencies in the VLF to MF bands (c.f., Herman, 1978), but since operational frequencies lower than ionospheric cutoff would be impractical, magnetospheric noise is unimportant here.

Next to galactic background, discrete noise sources such as certain radio stars (e.g., Cygnus A; Cassiopeia A) and the disturbed Sun can be troublesome under certain conditions. Specifically, intense noise may result when a discrete source falls within the main lobe of a narrow-band antenna, and to a lesser extent when within a side or back lobe. Without making any astronomical calculations, however, we would guess the fraction of time any of these sources were within a lobe would be small. The amplitude spectra of these various natural sources are given in section 5.4 for comparison with the desired lightning source spectrum.

## 5.3 Man Made Noise in Near Space

Sources classified as man made (Fig. 1) can be grouped as unintentional (including "incidental") and intentional. The former group comprises city noise, which in the worst case would be comparable to the magnitude of "Urban Noise" as predicted by Spaulding and Disney (1974), corrected for distance to the satellite. In the geosynchronous orbit, major cities falling within the antenna beam would contribute only about -52 dBk$T_o$b at 30 MHz, which would be about 70 dB below galactic background at that frequency. Moreover, as the spectrum of man made noise power falls off by about 28 dB per decade of frequency compared to only 23 dB for cosmic noise, the difference would be even greater at higher frequencies than 30 MHz. It may be safely concluded, therefore, that unintentional man made noise would be insignificant for an rf lightning sensor in geosynchronous orbit. Intentional sources,

however, are a different matter.

For a geosynchronous satellite positioned over 143 $^{o}$W, the expected interference due to terrestrial transmitters in the range 117-155 MHz is illustrated in Fig. 28. This prediction may not be very accurate because it is based on the distribution, number and power ratings of registered transmitters only, and the data base may otherwise be incomplete (Herman, 1978). Cosmic noise is significant only in the relatively empty band near 146 MHz. Overall, the predicted signal level averages about 15-20 dB above cosmic noise. It will be seen later (section 5.4) that this level is comparable to that expected from a solar flare on a disturbed Sun, and is thus likely to exceed the amplitude of a sferic observed at geosynchronous altitude. Detection of a sferic on an occupied frequency in this range would therefore be extremely unlikely.

These high signal levels can be expected to be maximum over populated areas where transmitters are in use for communication, broadcast, radar, and other purposes. An example of this is given in Fig. 29, which shows the geographical distribution of 466 MHz signals at 1100 km as measured by the Nimbus 4 satellite. As expected, the strongest signal power, equal to or greater than -110 dBm, is found over land areas. Other satellite measurements in the VHF/UHF bands include the LES-5 observations on frequencies from 253 to 284 MHz in a subsynchronous orbit at 33,400 km, which ultimately surveyed the whole subpolar globe as the craft drifted over a 9-month period (Haber et al, 1976). The strongest signals, ranging from about -110 dBm to -90 dBm, were observed to be coming from the U.S. on frequencies between 254 MHz and 262 MHz.

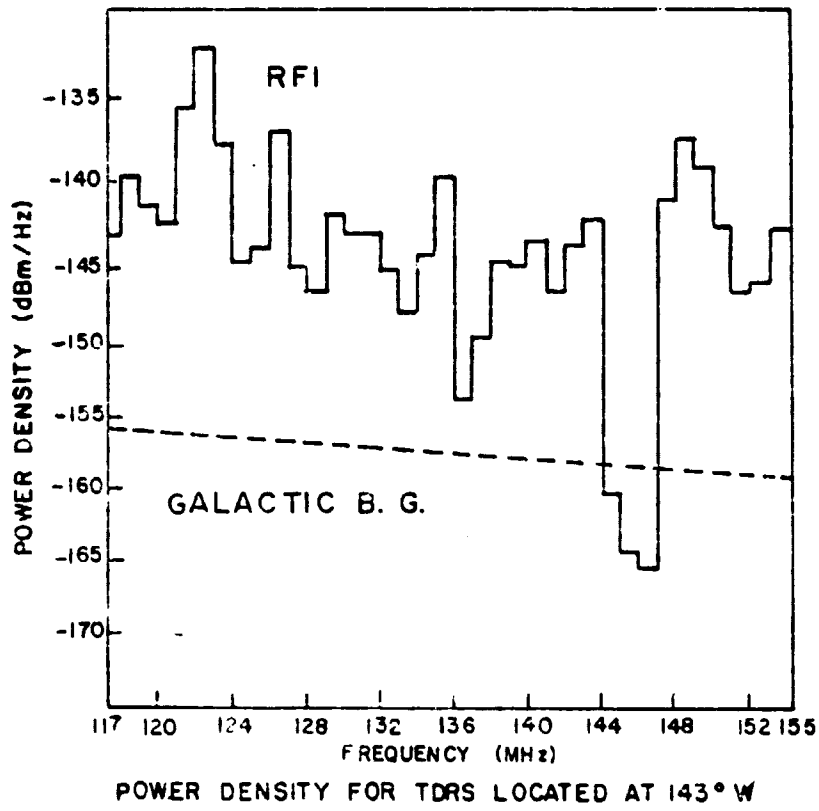


Fig. 28. Predicted rf interference due to terrestrial transmitters for a geosynchronous-orbit satellite over 143 $^{o}$W longitude (Herman, 1978).

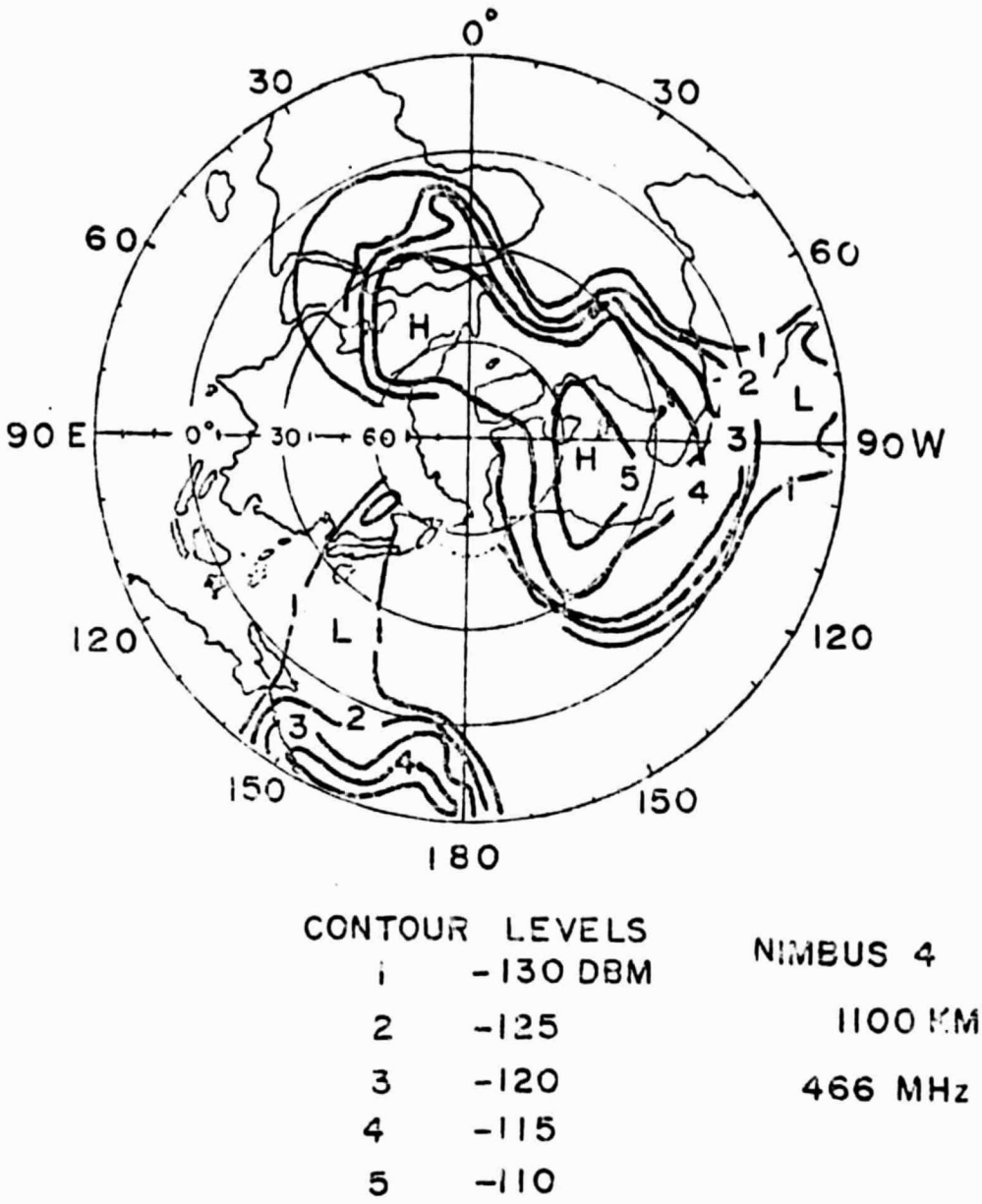


Fig. 29. Measured distribution of 466-MHz interfering signal power at 1100-km altitude (Herman, 1978).

Additionally, two strong signals were observed in the band 276-279 MHz. Similar results were found over Europe. The signal levels were 5 to 10 dB lower when the satellite was over South and Central America with the lower part of North America in view. By comparison, galactic background on these frequencies is on the order of -160 dBm, so transmitted signals on occupied frequencies in the VHF/UHF bands can be 50 dB and more above the cosmic noise level. Other measurements (reviewed by Herman, 1978) indicate similar levels of transmitted signals received in near space.

It is thus patently obvious that any rf lightning sensor designed for operation at geosynchronous height must utilize frequencies in unoccupied bands. To be safe, they should be chosen in bands which are not only unoccupied but also protected by international agreement. The radio astronomy protected bands as listed in Table 2 would offer reasonable choices. However, before a final design is frozen, the latest agreements sanctioned by the International Telecommunication Union should be checked to verify which frequencies are still under protection.

Table 2. Radio Frequency Bands Protected for Radio Astronomy Purposes (FCC, 1974).

| | | | |
|---|---|---|---|
| 73.00 - 74.60 | MHz | 2.69 - 2.700 | GHz |
| 406.1 - 410.0 | MHz | 4.990 - 5.000 | GHz |
| 1400 - 1427 | MHz | 10.68 - 10.70 | GHz |
| 1660 - 1670 | MHz | 15.35 - 15.40 | GHz |

## 5.4 Lightning Signal to Noise Ratio for Geosynchronous Orbit

Given that operational frequencies are free of interfering signal transmissions, the limiting factor in detectibility is provided by natural noise. To gain an estimate of the comparative noise power levels of natural sources vis a vis a lightning flash as a function of frequency, the lightning field intensity ($E_n$) spectral amplitude plotted in Fig. 27 has been converted to noise power ($F_a$) using the following formula (c.f., Herman, 1979):

$$F_a = E_n - 20(\log_{10} f_{MHz}) - 10(\log_{10} b) + 95.5 \qquad (12)$$

where $F_a$ is in dB$kT_o b$; that is, in dB above $kT_o b$, which is the noise power available from a dummy antenna at a temperature of $T_o$. Here, k is Boltzmann's constant and b is the bandwidth in hertz. Also, $f_{MHz}$ is the operating frequency expressed in megahertz and $E_n$ is in dB above 1 $\mu$V/m. The results are given in Fig. 30 for comparison with spectra from one of the most intense radio stars (Cassiopeia A), the radiation from the Sun for quiet and disturbed conditions, the transient burst of rf energy accompanying a large solar flare, and galactic background noise.

Somewhat surprizingly, the average lightning spectrum amplitude exceeds cosmic noise background over the whole frequency range considered, though the excess does diminish with increasing frequency. An earlier comparison using the Oh (1969) theoretical spectrum simply translated to geosynchronous distance indicated that the sferic amplitude would exceed galactic background only on frequencies below 400 MHz

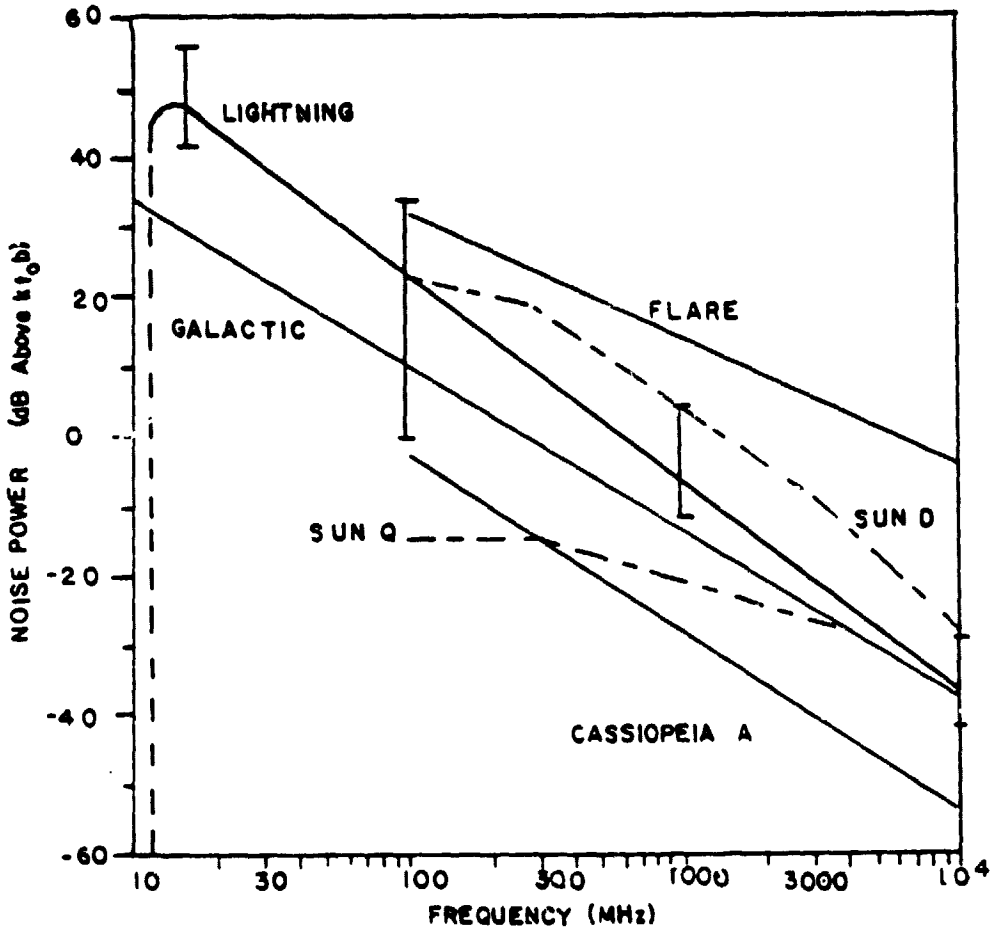


Fig. 30. Amplitude spectra of galactic background noise, the quiet (Q) and disturbed (D) Sun, a large solar flare from a greatly disturbed Sun, and a radio star (Cassiopeia A), compared to the lightning spectrum expected at geosynchronous height.

(Herman, 1980). By contrast, the average amplitude at 400 MHz in Fig. 30 is still 9 dB above galactic background, and is exceeded only by the radiation from a large flare and the disturbed Sun. On the optimistic side, the sferic power could be the order of 20 dB above cosmic noise power level on 400 MHz, but for a weak sferic the amplitude could be at or below this level. As noted earlier (section 5.1), it would be helpful to know what fraction of the rf sferics would be on the low side in order to assess the failure rate of detection from geosynchronous orbit.

Approaching 10 GHz (Fig. 30) , the average sferic amplitude is about the same as cosmic noise background and the quiet Sun, and it falls gradually below these power levels above 10 GHz. Considering that atmospheric absorption due to water vapor and oxygen begins to be perceptible at 10 GHz and increases rapidly with increasing frequency above that (Guidice, 1967), it appears that 10 GHz would be the upper limit for practical consideration for rf detection of lightning from space.

## 6. CONCLUSIONS

The foregoing modest investigation leads us to conclude that an rf sensor aboard a geosynchronous spacecraft would be able to detect lightning pulses on frequencies higher than is usually supposed, that is, out to a few GHz.

There would be some advantages to operating on frequencies in the higher ranges, say near 1400-1700 MHz, where ionospheric absorption, refraction and dispersion are negligible, and two radio astronomy protected bands are available (see Table 2). Here, the amplitude of the sferic may exceed cosmic noise background by about 5 to 15 dB or more, though weak sferics might be lost in the noise. Also, in this range and upward the structure of the sferic is similar to that at VLF; that is, discrete pulses associated with specific parts of the lightning discharge process; which is in contrast to the nearly continuous radiation in the HF and lower VHF part of the spectrum. With discrete pulses, direction finding techniques would be easier to apply, and smaller directive antennas would become feasible in the upper UHF band.

Even with directive antennas with narrow beam width ($\frac{1}{2}^{o}$, say), the resolution for pinpointing lightning locations from space will be poor, unless interferometric techniques can be developed.

An alternative band of operating frequencies could be chosen in the protected radio astronomy band at 406.1-410.0 MHz. Ionospheric effects here are still relatively unimportant, and the expected lightning signal would be perhaps 10-20 dB greater than cosmic noise. Again, weak sferics would be near the noise level, and if the disturbed Sun

were in the antenna beam it could constitute a serious temporary interference source.

With regard to ionospheric scintillations, consideration of the relative proximity of the transmitter (i.e., the lightning flash) and receiver to the diffraction screen creating the amplitude fluctuations seems to show that the effects will be small. This is so because one cannot assume reciprocity of propagation in the scintillation process. In general, the closer the source is to the diffraction screen, the smaller will be the fluctuation amplitude.

Finally, we stress again that observations must be carried out on unoccupied frequencies, since the amplitudes of deliberate rf transmissions will, as a general rule, far exceed the strength of a lightning rf pulse received in near space. Pulsed radars would be a particularly insidious source of interference. It is thus mandatory that any contemplated measurements be carried out in protected portions of the rf spectrum.

## 7. REFERENCES


Baldwin, J.L., Climates of the United States, U.S. Government Printing Office, Washington, D.C., 1973.

Bruce, C.E.R., and R.H. Golde, The lightning discharge, J. Inst. Elec. Engrs., 88, 487-505, 1941.

Carru, H., R. Gendrin, and M. Reyssat, La refraction ionospherique sur 20, 40 et 108 Mhz et son application a l'effet Doppler des satellites, Space Research, Proc. 1st Internatl. Space Science Symposium, (H. Kallman, ed.), North-Holland Publ. Co., Amsterdam, 286-303, 1960.

Chalmers, J.A., Atmospheric Electricity, Second Edition, Pergamon Press, Oxford, 1967.

Chiburis, R.L., and R.D. Jones, Severe storm observations from the Vela 4B satellite, in Proc. Waldorf Conf. on Long-Range Geographic Estimation of Lightning Sources, NRL Rpt. 7763, Naval Research Laboratory, Washington, D.C., p. 264, 1974.

Christensen, L.S., W. Frost, and W.W. Vaughan, Proceedings: Workshop on the Need for Lightning Observations from Space, University of Tennessee Space Institute, Tullahoma, Tennessee, 1979.

Davies, K., Ionospheric Radio Propagation, U.S. Government Printing Office, Washington, D.C., 1965.

Dennis, A.S., and E.T. Pierce, The return stroke of the lightning flash to Earth as a source of VLF atmospherics, Radio Sci. J. Res. NBS, 68D, 777-794, 1964.

FCC, Rules and Regulations of the Federal Communications Commission, Revised, U.S. Government Printing Office, Washington, D.C., 1974.

Goodman, J.M., Effect of the Ionosphere on Space Systems and Communications, U.S. Naval Research Laboratory, U.S. Government Printing Office, Washington, D.C., 1975.

Goodman, J.M., Effects of the Ionosphere on Space and Terrestrial Systems, U.S. Naval Research Laboratory, U.S. Government Printing Office, Washington, D.C., 1978.

Guidice, D.A., Radio Astronomy: A Revision of Chapter 22, Handbook of of Geophysics and Space Environments, Air Force Surveys in Geophysics No. 199, AFCRL-67-0621, 1967.

Haber, F., R.M. Showers, C. Kocher, and L.A. Forrest, Jr., Space Shuttle Electromagnetic Environment Experiment Phase A: Definition Study, The Moore School of Electrical Engineering, Philadelphia, Pa., Contractor Rpt., NASA CR-2707, June 1976.

Hart, W.C., and E.W. Malone, Lightning and Lightning Protection, Vol. IV, Multi-Volume EMC Encyclopedia Series, Don White Consultants, Inc., Gainesville, Virginia, 1979.

Herman, J.R., Spread F and ionospheric F-region irregularities, Rev. Geophys., 4, 255-299, 1966.

Herman, J.R., Earth as a Planetary Radio Noise Source, Final Rpt. to Avco Corp. on Contract NAS5-24007-Mod 4, 30 May 1974.

Herman, J.R., The radio noise environment in near space: a review, IEEE Proc. Internatl. Symp. on Electromagnetic Compatibility, Atlanta, p. 339, 1978.

Herman, J.R., Electromagnetic Ambients and Man-Made Noise, Vol. III, Multi-Volume EMC Encyclopedia Series, Don White Consultants, Inc., Gainesville, Virginia, 1979.

Herman, J.R., Noise sources in near-space spectrum pollution, in Proc. International Wroclaw Symposium on Electromagnetic Compatibility, (D.J. Bem, ed.), Wroclaw Tehcnical University, Wroclaw, Poland, 93-102, 1980

Herman, J.R., J.A. Caruso, and R.G. Stone, Radio Astronomy Explorer (RAE)-1. observations of terrestrial radio noise, Planet. Space Sci., 21, 443-461, 1973.

Hewitt, F.J., Radar studies of sources of noise in lightning, in Radio Noise of Terrestrial Origin, (F. Horner, ed.), Elsevier Publ. Co., Amsterdam, 72-84, 1962.

Hill, R.D., Electromagnetic radiation from the return stroke of a lightning discharge, J. Geophys. Res., 71, 1963-1967, 1966.

Horner, F., A review of information on atmospherics from near lightning discharges, in Monograph on Radio Noise of Terrestrial Origin, (F. Horner, ed.), Elsevier Publ. Co., Amsterdam, p. 85, 1962.

Horner, F., Radio noise in space originating in natural terrestrial sources, Planet. Space Sci., 13, 1137-1150, 1965.

Horner, F., and R.B. Bent, Measurement of terrestrial radio noise, Proc. Roy. Soc. A 311, p. 527, 1969.

Israël, H., Atmospheric Electricity, Vol. II, Fields, Charges, Currents, (Engl. Trans.), Israel Program for Scientific Translations, Jerusalem, 1973.

Kolokolov, V.D., Thunderstorm activity on the basis of instrument observations, Leningrad Main Geophysical Observatory Transactions No. 225, 3-15, 1968.

Lawrence, R.S., C.G. Little, and J.A. Chivers, A survey of ionospheric effects upon earth-space radio propagation, Proc. IEEE, 52, 4-27, 1964.

LeVine, D.M., Sources of the Strongest RF Radiation from Lightning, Goddard Space Flight Center, NASA Tech. Memo. 80265, 1979.

LeVine, D.M., and E.P. Krider, The temporal structure of HF and VHF radiations during Florida lightning return strokes, Geophys. Res. Lett., 4, 13, 1977.

Little, C.G., W.M. Rayton, and R.B. Roof, Review of ionospheric effects at VHF and UHF, Proc. I.R.E., 44, 992-1018, 1956.

Lundquist, S., Observed radiation pulses from lightning and the localization of thunderstorms in Sweden, in Proc. International Wroclaw Symposium on Electromagnetic Compatibility, (D.J. Bem, ed.), Wroclaw Technical University, Wroclaw, Poland, 657-662, 1980.

Mullen, J.P., A. Bushly, J. Lanat, and J. Pantoja, Gigahertz scintillation at the magnetic equator, in Effect of the Ionosphere on Space and Terrestrial Systems, (J.M. Goodman, ed.), Naval Research Laboratory, Washington, D.C., p. 31, 1978.

Oetzel, G.N., and E.T. Pierce, Radio emissions from close lightning, in Planetary Electrodynamics Vol I, (S.C. Coroniti and J. Hughes, eds.), Gordon and Breach Publishers, New York, p. 543, 1969.

Oh, L.L., Measured and calculated spectral amplitude distribution of lightning sferics, IEEE Trans. EMC, EMC-11, 125, Nov. 1969.

Pierce, E.T., The Counting of Lightning Flashes, Stanford Research Institute, Special Technical Rpt. 49, 1968.

Pierce, E.T., Sferics, in Atmospheric Exploration by Remote Probes, Vol. 2, p. 595, 1969.

Rufenach, C.L., Power-law wavenumber spectrum deduced from ionospheric scintillation observations, J. Geophys. Res., 77, 4761, 1972.

Rust, W.D., P.R. Krehbiel, and A. Shlanta, Measurements of radiation from lightning at 2200 MHz, Geophys. Res. Lett., 6, 85, 1979.